UNIVERSIDAD DE CONCEPCIÓN
FACULTAD DE CIENCIAS FÍSICAS Y MATEMÁTICAS

UNDERSTANDING THE IMPACT OF BINARY MASS TRANSFER IN THE ACCRETOR'S MEASURABLE PARAMETERS

Comprendiendo el impacto de la transferencia de masa en estrellas binarias sobre los parámetros observables de la estrella accretora.

By: Magdalena Vilaxa Campos

Thesis presented to the Faculty of Physical Sciences and Mathematics of the University of Concepción to obtain the degree of Master in Astronomy

April 2025
Concepción, Chile

Advisor: Dr. Nathan Leigh

A mi familia

AGRADECIMIENTOS

Quiero primeramente agradecer a mi familia: a mis padres, Paola y Leonel, por su cariño y todo el apoyo que me han prestado a lo largo de mi vida, y en particular durante mi vida académica. Me brindaron sustento durante todos estos años, gracias a lo cual pude sacar adelante este trabajo. A mi hermana *Chichi* que me acompañó durante los años de pandemia. Doy gracias a mi *Yaya*, a Uhura y Teodoro quienes son grandes fuentes de alegría cada vez que visito a mi familia. Agradezco además a mi novio Vicente, cuya compañía ha sido clave en mis tiempos más difíciles. A pesar de sus obligaciones siempre halló un tiempo para cuidarme. No dejo de dar las gracias por todo el cariño que me ha dado.

Doy gracias a mis compañeros tesistas de la sala 112 por aceptarme pues jamás me sentí fuera de lugar en este espacio de trabajo. Destaco en particular a Vanessa, mi vecina de escritorio y amiga, por escucharme y aconsejarme. Durante mi periodo de estudiante de Magister tuve también el agrado de reencontrarme con mi querida amiga Cielo quien me ayudó mucho con su cariño y validación. Aprecio además los momentos de esparcimiento con mi amiga *Connie*.

La ayuda de Marcela, Secretaria del Departamento de Astronomía de la Universidad de Concepción, han sido invaluable en este proceso y estaré siempre agradecida por su disposición. Doy gracias también a todas las personas del Instituto Anton Pannekoek (API) de la Universidad de Ámsterdam y del equipo de investigación del Dr. Robert D. Mathieu de la Universidad de Wisconsin-Madison con las que tuve la oportunidad de conversar. Sus diversas perspectivas reavivaron mi interés por la ciencia en varios momentos de estancamiento.

Reconozco el apoyo financiero entregado por el Núcleo Milenio en Tecnología e Investigación Transversal para explorar Agujeros Negros Supermasivos (TITANs).

Finalmente, agradezco a mis *idols* favoritas Fruits Zipper, Babymetal y Miku Hatsune por animarme con su música cuando las necesité.

Resumen

Las estrellas en sistemas binarios o de orden mayor pueden vivir eventos de transferencia de masa entre sus componentes. El momento angular transferido a la estrella accretora por medio de la masa ganada puede afectar los parámetros observables de la estrella y acelerar su rotación hasta una velocidad crítica. En el caso de accreción a través de un disco de accreción, se espera que una ganancia de masa menor al 10% de la masa inicial de la accretora la lleve a su velocidad de rotación crítica y la destruya.

En este trabajo buscamos explorar el efecto que un *stream* de masa tiene en la rotación de la accretora como un posible mecanismo que permita a la estrella accretora ganar más de una décima parte de su masa inicial sin ganar el momentum necesario para llevar a a rotación crítica

Presentamos aquí un nuevo modelo analítico para caracterizar los efectos de la accreción directa en los parámetros medibles de la accretora, en función del semi-eje mayor y eccentricidad del sistema y la velocidad de rotación de la estrella donante. Este modelo aborda el problema como un problema de dos cuerpos, donde un *stream* de masa está compuesto por múltiples partículas discretas que no interactúan entre ellas y que sólamente son influenciadas por el potencial gravitatorio de la accretora. Cada partícula tiene una solución orbital instantánea derivada a partir de sus condiciones iniciales. La contribución de cada partícula a la aceleración de la velocidad rotacional de la accretore está dada por la componente tangencial de la velocidad de impacto a través de la conservación de momento angular.

Hallamos que la accreción directa demuestra ser menos eficiente en acelerar la estrella accretora en relación a la accreción por disco, y por lo tanto permite a la estrella ganar una mayor fracción ($> 10\%$) de su masa inicial sin alcanzar rotación crítica. Además, cuantificamos la fracción de masa que impacta a la accretora directamente en contraste a aquella que es expulsada del sistema o forma un disco al rededor de la accretora.

Keywords – Binarias, accreción, dinámica estelar

Abstract

Stars in binaries and higher order systems can experience mass transfer events between their components. The angular momentum carried by the mass gained by the accretor can change the observable parameters of the star and spin it up to critical rotation. In the case of disk accretion, a mass gain lesser than a 10% of the accretor's initial mass is expected to bring it to a critical rotation rate and break it apart.

In this work, we aim to explore the spin-up effect of direct accretion through a stream as a possible mechanism for an accretor to gain more than a tenth of its mass without gaining enough momentum to reach critical rotation.

Here, we present a novel analytical model to characterize the effects of direct mass transfer in the accretor's measurable parameters as a function of the binary's semi-major axis and eccentricity and the donor's rotational velocity. This model takes a two-body approach to the problem, where a stream is decomposed as many discrete particles that do not interact with each other and are influenced by only the accretor's gravitational potential. Each parcel has an instant orbital solution derived from its initial conditions. The contribution each accreted parcel has to the total spin-up of the accretor is given by its tangential velocity at impact, through conservation of angular momentum.

We find that direct mass transfer proves to be less efficient at spinning up the accretor than an accretion disk and thus enables the star to gain a greater fraction ($>$10%) of its initial mass without reaching critical rotation. In addition, we quantify the fraction of mass that directly impact the accretor in contrast to the mass that is either lost from the system or creates a disk around the star.

Keywords – Binaries, accretion, stellar dynamics

Contents

AGRADECIMIENTOS i

Resumen ii

Abstract iii

1 Introduction 1

2 Methods 3
2.1 The Model . . . 3
2.2 Validation of Assumptions . . . 9
2.2.1 3-body problem . . . 9

3 Results 18
3.1 Spin-up . . . 18
3.1.1 Semi-major axis a . . . 18
3.1.2 Eccentricity e . . . 22
3.1.3 Donor's rotation . . . 24
3.2 Conservativeness . . . 25
3.2.1 Semi-major axis a . . . 25
3.2.2 Eccentricity e . . . 26
3.2.3 Donor's rotation . . . 28
3.3 Mass ratio q . . . 28
3.4 Timescale . . . 29
3.5 L1 . . . 30

4 Discussion 32
4.1 Synchronization . . . 32
4.2 Evolution of orbital parameters . . . 36
4.2.1 Semi-major axis a . . . 36
4.2.2 Eccentricity e . . . 37
4.3 Disk formation . . . 38

5 Conclusion 39

References 42

Apéndices **46**

A Apendix **46**
A1 Limits on v_{extra}/v_{per} 46
A2 Eccentricity and angular momentum 48

List of Tables

2.2.1 Best fit polynome coefficients 12

4.1.1 Synchronization ($e = 0.00$) and pseudo-synchronization ($e > 0.00$) times for systems with $a = 1.23$ & 2.30 and $e = 0.00$, 0.30, 0.70 & 0.80, extracted from figure 8 of Moreno et al. (2011). All systems have $\beta_0 = 1.2$ ($v_{\text{extra}}/v_{\text{per}} = 0.73$). 36

List of Figures

2.1.1 Diagram of the system. The accreting star's position is fixed to the origin of the reference frame while the donor star, of mass m_{don}, orbits around it. A parcel of mass, located at a distance r_{L1} from the accretor's center of mass, is let go with an initial velocity $\vec{v}_i = \vec{v}_{orb} + \vec{v}_{extra}$. 4
2.1.2 Inclination of a parcel's orbit (blue) with respect to the donor's orbit (in the same direction of the gray dashed $L1$ position). Angle θ in red represents the true anomaly of the starting point of a parcel with respect to the donor's orbit while θ_p in blue represents the true anomaly of the parcel's starting point with respect of the parcel's orbit. 6
2.1.3 Resulting velocity $\vec{v}_i$ for a parcel in the first half (top) and the second half of the donor's orbit (bottom). Top panel: $\vec{v}_{extra}$ always points outwards with respect to the L1 orbit. This produces an initial angle α_i that is always greater than α_{orb}. Bottom panel: $\vec{v}_{extra}$ always points inwards with respect to the L1 orbit. This produces an initial angle α_i that is always smaller than α_{orb}. . . . 7
2.2.1 Value of $v_{\text{extra}}/v_{\text{orb}}$ for which the impact angle α_{imp} becomes 0, as a function of the mass ratio q, for systems with $a = 1.30$, 1.80 & 2.20 AU (red, yellow and green respectively). The open circles show the resulting value from a three-body approach while the solid lines plot the best fit, described by equation 2.2.10. 13
2.2.2 Angular rotational speed of the donor, in terms of the angular orbital velocity of the binary system, as a function of $v_{\text{extra}}/v_{\text{orb}}$. Here, it is assumed that the donor's radius is equal to $a - r_{L1}$. . . 14
2.2.3 Amplitude A, as a function of the semi-major axis a, for systems with $q = 0.50$, 0.75, 1.00, 1.25 & 1.50 (red, yellow, green, blue and pink respectively). The open circles show the resulting value from a three-body approach while the solid lines plot the best fit, described by equation 2.2.11. 16

2.2.4 Impact velocity in a logarithmic scale (top) and angle (bottom) for systems of an orbital separation $a = 1.30$, 1.80 & 2.20 au (red, yellow & green) as a function of v_{extra}/v_{orb}. The data corresponding to our model (solid lines) has been corrected through equation 2.2.13 to better approximate the three-body results (open circles). Only data where $v_{\rm extra}/v_{\rm orb} < \frac{v_{extra}}{v_{orb}}(\alpha_{imp} = 0)_{3b}$ is displayed. . . . 17

3.1.1 Spin-up of the accretor star in terms of its critical rotational velocity after one orbital period, as a function of the binary system's semi-major axis a. Left: All systems have $v_{\rm extra}/v_{\rm per} = 0.90$ and e takes the values 0.00, 0.05, 0.10, 0.30 & 0.60, shown by different colors (red, yellow, green, blue and pink). Right: All systems have $e = 0.1$ and $v_{\rm extra}/v_{\rm per}$ takes the values 0.80, 0.85, 0.90, & 0.95 (red, yellow, green and blue). 19

3.1.2 Semi-major axis value for maximum spin-up of the accreting star as a function of the system's eccentricity with constant $v_{\rm extra}/v_{\rm per} = 0.90$ (left) and the donor's rotation with constant $e = 0.10$ (right). The shaded region marks the range of a we work with in the analysis. 20

3.1.3 Graphic representation of cases 1 and 2, of the eccentricity spin-up analysis. The accretor star is depicted by a pink circle whose size has been scaled by a factor of 10. A dotted line draws the orbit of the donor's center of mass and, from widest to narrower, the blue, green and purple regions represent areas of the orbit where conditions 1, 2 and 3 are met, respectively, while the black region represents the intersection of all three. Case 1 is exemplified by the yellow curve ($a = 1.80$ AU) on the left panel of figure 3.1.4, and goes contains stages a_1, b_1 and d for increasing eccentricities. Case 2 is exemplified by the green curve ($a = 2.20$ AU) on the left panel of figure 3.1.4, and goes contains stages a_2, b_2, c and d for increasing eccentricities. 21

3.1.4 Spin-up of the accretor star in terms of its critical rotational velocity, as a function of the binary system's eccentricity e. Left: All systems have $v_{\rm extra}/v_{\rm per} = 0.90$. The result is displayed for $a = 1.30$, 1.80 & 2.20 AU (red, yellow and green). Right: All systems have $a = 1.80$ AU and $v_{\rm extra}/v_{\rm per}$ takes the values 0.80, 0.85, 0.90, & 0.95 (red, yellow, green and blue). 22

3.1.5 Spin-up of the accretor star in terms of its critical rotational velocity, as a function of the donor's rotational velocity $v_{\rm extra}/v_{\rm per}$. Left: All systems have $e = 0.10$. The result is displayed for $a = 1.30$, 1.80 & 2.20 AU (red, yellow and green). Right: All systems have $a = 1.80$ AU and e takes the values 0.00, 0.05, 0.10, 0.30, & 0.60 (red, yellow, green, blue and pink). 24

3.2.1 Conservativeness of the accretion event, as a function of the binary system's semi-major axis a. Left: All systems have $v_{\rm extra}/v_{\rm per} = 0.90$. The result is displayed for $e = 0.00$, 0.05, 0.10, 0.30 & 0.60 (red, yellow, green, blue and pink). Right: All systems have $e = 0.10$ and $v_{\rm extra}/v_{\rm per}$ takes the values 0.80, 0.85, 0.90 & 0.95 (red, yellow, green and blue). 26
3.2.2 Conservativeness of the accretion event, as a function of the binary system's eccentricity e. Left: All systems have $v_{\rm extra}/v_{\rm per} = 0.90$. The result is displayed for $a = 1.30$, 1.80 & 2.20 AU (red, yellow and green). Right: All systems have $a = 1.80$ AU and $v_{\rm extra}/v_{\rm per}$ takes the values 0.80, 0.85, 0.90, & 0.95 (red, yellow, green and blue). 27
3.2.3 Conservativeness of the accretion event, as a function of the donor's rotational velocity $v_{\rm extra}/v_{\rm per}$. Left: All systems have $e = 0.10$. The result is displayed for $a = 1.30$, 1.80 & 2.20 AU (red, yellow and green). Right: All systems have $a = 1.80$ AU and e takes the values 0.00, 0.05, 0.10, 0.30, & 0.60 (red, yellow, green, blue and pink). . 28
3.3.1 Alike figure 3.1.1 but for $q = 0.50$, 0.75, 1.00, 1.25 & 1.50 and constant $e = 0.10$ and $v_{\rm extra}/v_{\rm per} = 0.90$. 29
3.5.1 Akin to figure 2.2.2 except here the $L1$ calculation does not include the term for centripetal force. 31

4.1.1 Ratio of orbital angular momentum to rotational angular momentum at the equillibrium state for a range of values of parameter $v_{\rm extra}/v_{\rm per}$. All sistems have $a = 1.80$ AU. Curves for $e = 0.00$, 0.05, 0.10, 0.30 & 0.60 (red, yellow, green, blue & pink) are displayed. It is important to note that we only display the $e = 0.60$ data for $v_{\rm extra}/v_{\rm per} < 2$ due to numerical errors related to the computation of $L1$ that were affecting the results. 34
4.1.2 Akin to figure 2.2.2 but for pseudo-synchronicity. The dashed line and solid black line represent the lower and upper limits for a pseudo-synchronous state (0.8 & 1 respectively). Like in figure 4.1.1, data for $e = 0.60$ is not displayed beyond $v_{\rm extra}/v_{\rm per} = 2$ because of numerical issues related to the resolution in the computation of $L1$. 35

A1.1 Caption 47

Chapter 1

Introduction

Stars do not always live in isolation. About 85% of all stars have at least one companion (Offner et al., 2023) and, in particular, 46% of solar type stars are part of binaries or higher order multiple star systems (Raghavan et al., 2010).

Throughout their lives, binaries and higher order systems might experience accretion events between their components, typically referred to as the accretor and donor. Mass transfer can occur through different mechanisms depending on the binary's conditions, for example, closer systems might accrete through wind Roche lobe overflow (WRLOF) while systems with wider orbits accrete through Bondi-Hoyle (BH) accretion (Chen et al., 2017).

Mass transfer events can affect the orbital parameters of the system (Sepinsky et al., 2007, 2009, 2010) as well as the composition (McClure, 1984) and observational properties (i.e. color, brightness, rotational velocity) of the accretor. However, the changes to an accreting star's observational properties due to the increase in mass are yet to be fully understood.

Blue Stragglers (BSs) are stars that, if members of a cluster, are found in the region brighter and bluer than the main-sequence turn-off (TO) in the color-magnitude diagram (CMD). These stars were first observed in the globular cluster M3 by Sandage (1953) and are thought to be the product of mass transfer events (Mathieu and Geller, 2009; Portegies Zwart and Leigh, 2019). BSs not only can form within binaries but pairs of BSs can also form through accretion from an outer tertiary (Leigh et al., 2020).

Packet (1981) estimated that only 10% of a star's initial mass would need to be accreted by it to spin it up to its critical rotation rate (i.e. the critical angular velocity at which the star reaches centrifugal limit at the equator and can not longer hold itself together) therefore breaking up the star at its outer layers. This would make most accretion products rapid rotators. Rapidly rotating stars are rare, but some have recently been identified in globular culsters via their blue straggler populations. Specifically, rapid rotators seem to prefer low-density cluster environments (Ferraro et al., 2023) where wider systems have a higher survival rate due to the lower frequency of strong dissociative dynamical interactions between systems.

Sepinsky et al. (2010) approached modelling direct accretion through three-body integration. In their approach, the donor star looses a small discrete amount of mass strictly at periastron passage, resulting in either self-accretion, direct impact or possibly disk formation. Their results focuss on how the mass transfer event affects the orbital parameters as well as the donor's rotation rate with respect to the system's mean motion.

In their study, Dosopoulou and Kalogera (2016a) (and the continuation Dosopoulou and Kalogera (2016b)) track the evolution of the binary orbital elements in eccentric binary systems. Their computation treats mass transfer as a perturbation to the donor-accretor two-body system.

In this work we present a novel analytical model for direct accretion reducing the system to an accretor-particle two-body problem in section 2, where we also address the impact of neglecting the influence of the donor's potential (section 2.2). We measure the spin-up effect the accretor suffers due to mass gain after one orbital period as well as the efficiency of mass transfer, for a range of different semi-major axis lenghths, eccentricities and donor rotation rates (section 3). Finally, we discuss the timescales for orbital evolution and how they compare with our accretion timescales in section 4. We sumarize our findings in section 5.

Chapter 2

Methods

2.1 The Model

We consider a binary star where m_{don} and m_{acc} are the masses of the primary and secondary, or donor and accretor, respectively. The frame of reference is fixed to the accretor star so that the donor star traces an elliptical orbit around it. We denote by an "a" the binary initial semi-major axis, and the eccentricity by an "e".

The distance from the origin to the L1 point is so that, at that position, the gravitational effect of the donor, the gravitational effect of the accretor and the centripetal force inflicted over an imaginary particle of velocity v_i are in equated. This condition is met when equation 2.1.1 is fulfilled

$$\frac{Gm_{don}}{(a - r_{L1})^2} - \frac{Gm_{acc}}{r_{L1}^2} + \frac{v_i^2}{r_{L1}} = 0 \tag{2.1.1}$$

The L1 point moves as the donor orbits around the accretor. At every position along the L1 orbit, we imagine that a single parcel of mass is released from the donor's envelope. For this approach, the following assumptions are made:

I The in-falling parcel of mass is solely affected by the gravitational force the accretor star inflicts on it. The gravitational potential of the donor is not taken into account once a parcel is released.

II The effect of a stream of mass directly impacting the accreting star is

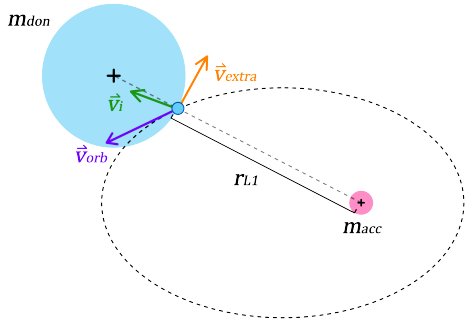

Figure 2.1.1: Diagram of the system. The accreting star's position is fixed to the origin of the reference frame while the donor star, of mass m_{don}, orbits around it. A parcel of mass, located at a distance r_{L1} from the accretor's center of mass, is let go with an initial velocity $\vec{v}_i = \vec{v}_{orb} + \vec{v}_{extra}$.

approximated by the superposition of every accreted parcel over a single orbital period of the system.

III Only the tangential component of a parcel's velocity at the moment of impact will contribute to the rotational energy of the accretor.

IV The radial component will instead contribute to the star's thermal energy.

It is important to highlight that this is a rough first-order approximation that we make in order to be able to derive analytic solutions. We quantify the validity of this assumptions later in Section 2.2 by comparing to existing or known solutions for this problem.

We take 1000 values for the true anomaly, equally separated in time over a single orbital period. The donor's orbit is computed from its orbital elements, so both the trajectory of the donor's center of mass and the distance to L1 are independent of the time-step size, therefore avoiding time-step related errors. At each position on the L1 orbit, a parcel is let go from the donor's envelope. Given our second assumption (II), we can now focus our analysis on a single parcel.

At a distance r_{L1} from the accretor's center, the parcel starts with an initial velocity $\vec{v}_i$, calculated as the instantaneous orbital velocity of the donor star's center of mass $\vec{v}_{orb}$ in addition to an extra velocity $\vec{v}_{extra}$ perpendicular to the radial direction, as depicted in Figure 2.1.1. The term $\vec{v}_{extra}$ acts as the donor's surface velocity from an angular rotational velocity $\omega_{don,rot}$. In order for $\vec{v}_{extra}$ to act opposite to the orbital motion at periastron, it is assumed that $\omega_{don,rot}$ and

the angular orbital velocity of the donor around the accretor ω_{orb} have the same direction. For eccentricities greater than 0, $\vec{v}_{orb}$ and $\vec{v}_{extra}$ are only parallel at periapsis and apoapsis, any other position in the orbit produces an initial velocity with an angle α_i, different than the orbital velocity's angle α_{orb}. A parcel's initial speed v_i and its corresponding angle α_i are given respectively by

$$v_i = \sqrt{v_{orb}^2 + v_{extra}^2 - 2|v_{orb}||v_{extra}| \cos\left(\frac{\pi}{2} - \alpha_{orb}\right)} \tag{2.1.2}$$

and

$$\alpha_i = \alpha_{orb} + \arcsin\left[\frac{v_{extra}}{v_i} \sin\left(\frac{\pi}{2} - \alpha_{orb}\right)\right] \tag{2.1.3}$$

We defer this calculation to an Appendix.

Having a value for the initial velocity and its angle with respect to the radial direction, a trajectory can be predicted for the parcel if we assume it will be in a Keplerian orbit around the accretor. The semi-major axis a_p of this orbit can be obtained through the Vis-viva equation

$$v = \sqrt{GM\left(\frac{2}{r} - \frac{1}{a}\right)} \tag{2.1.4}$$

, by solving for the semi-major axis

$$a_p = \left(\frac{2}{r_{L1}} - \frac{v_i^2}{Gm_{acc}}\right)^{-1} \tag{2.1.5}$$

The use of the Vis-viva equation to relate the particle's velocity to the semi-major axis of its orbit ensures the conservation of its mechanical energy. The eccentricity e_p can be obtained through

$$e_p = \frac{c_p}{a_p} \tag{2.1.6}$$

, where

$$c_p = \frac{1}{2}\sqrt{r_{L1}^2 + (2a_p - r_{L1})^2 - 2r_{L1}(2a_p - r_{L1}) \cos\left(\pi - 2\alpha_i\right)} \tag{2.1.7}$$

This approach is consistent with the conservation of angular momentum. An

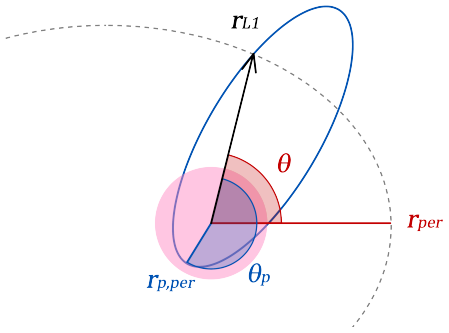

Figure 2.1.2: Inclination of a parcel's orbit (blue) with respect to the donor's orbit (in the same direction of the gray dashed $L1$ position). Angle θ in red represents the true anomaly of the starting point of a parcel with respect to the donor's orbit while θ_p in blue represents the true anomaly of the parcel's starting point with respect of the parcel's orbit.

extensive demonstration can be found in Appendix A2.

Here, the true anomaly of the initial position of the parcel with respect to the new orbit, assuming the accretor is at one of the trajectory's foci, is given by

$$\theta_p(t_p = 0) = \pi - \arcsin\left[\frac{2a_p - r}{2c_p}\sin\left(\pi - 2\alpha_i\right)\right]. \tag{2.1.8}$$

where it is important to note that the argument $t_p = 0$ denotes the initial position within the parcel's orbit and it is not an indicator of the time transpired since the beginning of the donor's orbit at periapsis. Equation 2.1.8, in combination with θ, the true anomaly of the starting point of the parcel in the L1 orbit, gives us the inclination of the parcel's orbit with respect to the donor's orbit, as shown in figure 2.1.2.

In order for a parcel to be considered as accreted it must fulfill the following conditions:

1. The donor star must be overfilling its Roche lobe for the system to undergo Roche lobe overflow (RLOF) accretion. We define the parameter f as the fraction of the donor's radius that protrudes beyond the L1 point at any point of the orbit. This assumes the donor as a rigid body. This value can be interpreted as the opening angle of the Roche surface for a teardrop-shaped donor in a more realistic scenario.

2. Given the initial velocity v_i and its angle with respect to the radial direction

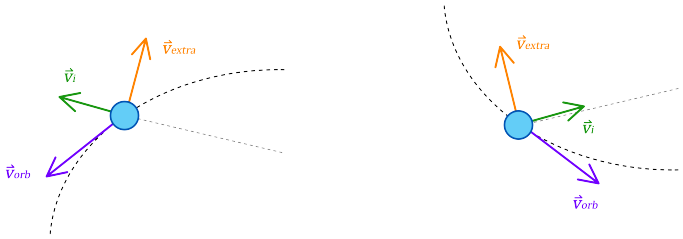

Figure 2.1.3: Resulting velocity $\vec{v_i}$ for a parcel in the first half (top) and the second half of the donor's orbit (bottom). Top panel: $\vec{v}_{extra}$ always points outwards with respect to the L1 orbit. This produces an initial angle α_i that is always greater than α_{orb}. Bottom panel: $\vec{v}_{extra}$ always points inwards with respect to the L1 orbit. This produces an initial angle α_i that is always smaller than α_{orb}.

α_i, the resulting trajectory must impact the accretor, given its radius. Impact is defined as the first point in the trajectory at which the distance from the particle to the center of the system is less than or equal to the accretor's radius. This is

$$r_p \leq r_{acc} \tag{2.1.9}$$

3. The angle of the initial velocity must be less than or equal to the angle of the orbital velocity α_{orb}. This discards any parcel whose initial velocity's direction pushes it back towards the donor star. This condition prevents any accretion from happening in the first half of the period, due to the resulting $\vec{v_i}$ always pointing outwards, as shown in Figure 2.1.3.

During a single orbital period, a flag is assigned to each timestep to indicate if the corresponding parcel was accreted (1) or not (0), in accordance with condition 2. In addition to the initial values, the velocity and angle at impact of each accreted parcel are stored

This experiment is repeated for many systems with a range of values for e, a and the velocity fraction v_{extra}/v_{per}. The latter describes the magnitude of the linear rotational velocity at the surface of the donor divided by the donor's linear orbital velocity at periastron passage. This way, v_{extra}/v_{per} is a measurement of the donor's rotation: when $v_{extra}/v_{per} = 0$ the donor star is non-rotating, while $v_{extra}/v_{per} = 1$ describes the case where the donor's surface rotation and its

orbital velocity at periastron are equal. When $v_{extra}/v_{per} = 1$, a parcel dropped at periastron passage will fall to the accretor with an initial speed $v_i = 0.0$.

Since the value of the overflow fraction f does not affect the trajectory of an in-falling parcel, this value is added to the dataset after all trajectories have been obtained. This also allows us to test the accretor's response to different values of f without running the experiment again. The value of this parameter can be obtained for every position in the L1 orbit as described by equation 2.1.10

$$f(\theta) = 1 - \frac{r_{orb}(\theta) - r_{L1}(\theta)}{r_{orb,per} - r_{L1,per}}(1 - f_{per}) \tag{2.1.10}$$

where f_{per} is the value of f at periastron.

All negative values (i.e. positions where the donor star does not overflow its Roche lobe) are replaced with 0 in the dataset so that they do not contribute to the total gained mass. At the same time this parameter is added to the datasets, condition 3 is evaluated and the accretion flag is updated to fulfil it.

Lastly, taking $\dot{M} = 10^{-6} M_{\odot}/yr$ (a mass transfer rate on the lower limit of the range Lajoie and Sills (2011) worked with) as the mass loss rate of our donor, the mass contained in each parcel of mass can be obtained as follows:

$$m_p(\theta) = \frac{\dot{M}T}{\sum_i f_i} f(\theta) \tag{2.1.11}$$

where T is the orbital period of the binary.

The routine makes use of AMUSE (Portegies Zwart and McMillan, 2018; Portegies Zwart et al., 2013; Pelupessy et al., 2013; Portegies Zwart et al., 2009) to introduce physical units into the calculation.

In the following section, the spin-up suffered by the accreting star due to the mass gain, in addition to the conservativeness of the accretion, are evaluated in terms of our four main parameters: semi-major axis "a", eccentricity "e", synchronicity "v_{extra}/v_{per}" and overflow fraction at periastron "f_{per}". For all cases the initial masses of both the accretor and donor were 1.00 $M_{\odot}$ and 1.20 $M_{\odot}$, respectively. Given that a circular orbit provides the longest distance from the accretor to periastron for a fixed length of the semi-major axis, we will work with a between

the lower limit where the surface of both stars are almost touching

$$\min(a) = 1.01 * (r_{acc} + \max(r_{AGB})) \tag{2.1.12}$$

and the upper limit

$$r_{orb}(e = 0) < r_{L1} + \max(r_{AGB}) \tag{2.1.13}$$

where $\max(r_{AGB})$ is the largest radius for a star of mass m_{don} during its asymptotic giant branch stage, in our case, $\max(r_{AGB}) = 263\ R_{\odot}$. This way, the lower limit represents a system where the stars' surfaces are almost touching, while the upper limit for the semi-major axis can be obtained through equation 2.1.1 by solving for a, setting $a = r_{L1} + \max(r_{AGB})$. This limit is set so there is always mass overflow at least at periastron.

In the case of the eccentricity, we choose values between 0.00 to 0.95 to cover the widest range possible. Values for v_{extra}/v_{per} ranged between 0.80 and 1.00 (see Appendix A1). Lastly, f_{per} was set to 0.1 for all tests. We expect a change in f_{per} would only scale up or down the total effect the mass gain causes on the accretor without changing the overall behaviour of the accretion.

2.2 Validation of Assumptions

2.2.1 3-body problem

Under the assumption that a parcel of mass is not affected by the gravitational potential of the donor beyond $L1$ reduces the problem from three bodies to just two. In this section, we compare our model to a planar restricted circular three-body problem. We choose this specific case of the three-body problem because it is the only one for which analytic equations of motion can be derived. Any other case requires to be solved numerically.

We will consider a donor of mass m_{don}, an accretor of mass m_{acc} and a parcel of negligible mass. The total mass of the stars in this system is taken as unity so that

$$m_{don} = \kappa \qquad \text{and} \qquad m_{acc} = 1 - \kappa \tag{2.2.1}$$

where κ is a constant. Additionally, the distance a between the stars is set as the length unit and the time unit is defined so that

$$\frac{P}{2\pi} = 1 \tag{2.2.2}$$

An inertial frame of reference of coordinate axes $\underline{x}$ and $\underline{y}$ is positioned with its origin at the center of mass between both stars, whith the donor and accretor at distances $1-\kappa$ and κ respectively. In addition, a rotating frame of reference of coordinate axes x and y is positioned so that x aligns with the line conecting the centers of mass of both stars. The frame rotates at a rate

$$\vec{\omega} = \sqrt{\frac{G(m_{acc}+m_{don})}{a^3}}\hat{y} = 1\hat{y} \tag{2.2.3}$$

Equation 5.10 of Valtonen and Karttunen (2006) describes the equations of motion in such system. In our terms, these equations become

$$\ddot{x} = \frac{\partial\Omega}{\partial x} + 2\dot{y} \qquad \text{and} \qquad \ddot{y} = \frac{\partial\Omega}{\partial y} - 2\dot{x} \tag{2.2.4}$$

where

$$\frac{\partial\Omega}{\partial x} = x + \frac{(\kappa-1)(\kappa+x)}{((\kappa+x)^2+y^2)^{3/2}} + \frac{\kappa(\kappa+x-1)}{((\kappa+x-1)^2+y^2)^{3/2}} \tag{2.2.5}$$

and

$$\frac{\partial\Omega}{\partial y} = y + \frac{(\kappa-1)y}{((\kappa+x)^2+y^2)^{3/2}} + \frac{\kappa y}{((\kappa+x-1)^2+y^2)^{3/2}} \tag{2.2.6}$$

The initial position of a particle dropped from the L1 point is

$$\vec{r_p} = (r_{L1}-\kappa)\hat{x} \tag{2.2.7}$$

where r_{L1} is the distance between the accretor and the particle, calculated through equation 2.1.1.

In order to compare this three-body simulation to our model as an independent check of the validity of our model assumptions, the massless particle must be given an additional initial velocity against the motion of the donor. Given that this

case describes circular motion between the stars, the orbital velocity of the donor and the added velocity are always parallel to each other and can be described by equation A1.9 where the donor's rotation is

$$\vec{v}_{don} = \vec{\omega} \times \vec{r}_{don} = |\vec{\omega}|(1-\kappa)\hat{y} \tag{2.2.8}$$

Now, correcting for the frame's rotation, we obtain

$$\begin{aligned} \vec{v_p} &= \left(1 - \frac{v_{extra}}{v_{orb}}\right) \vec{v}_{don} - \vec{\omega} \times \vec{r}_p \\ &= \left[\left(1 - \frac{v_{extra}}{v_{orb}}\right)(1-\kappa) - |\vec{r}_p|\right] \hat{y} \end{aligned} \tag{2.2.9}$$

Having set the initial conditions, the infall is simulated with a timestep $dt = 1$ minute untill one of the following three events occur: i) the particle approaches the accretor at a distance equal or lesser than the accretor's radius, ii) the particle reaches a distance from the accretor greater than the $L1$ distance, or iii) the particle continues to orbit around the accretor through the span of the system's orbital period.

Although the impact velocity for both our model and the three-body approach fall within the same order of magnitude, there are two significant diferences between the resulting impact angles. First, the three-body approach results are displaced towards higher donor rotation rates in comparison to our model. This is an effect of the donor's gravitational potential being considered in the former. As the donor orbits the accretor, it slightly pulls the parcel towards it, resulting in a wider orbit when compared to the same $v_{\text{extra}}/v_{\text{orb}}$ value in our model, therefore the donor has to spin faster then in our model in order to produce the same results. We see too that, in our model, α_{imp} equals 0 when $v_{\text{extra}}/v_{\text{orb}}$ equals 1, while in the three-body aproach there seems to be a small difference between systems with different orbital separations.

To find this displacement, the $v_{\text{extra}}/v_{\text{orb}}$ value for which the impact angle is zero is fit to a polynomial function for $a = 1.20$, 1.80 & 2.20 , in terms of the system's mass ratio q. The best fit polynome coefficients for each curve are showcased in table 2.2.1.

We then find a polynomial fit for the coefficients of each order, obtaining an

Table 2.2.1: Best fit polynome coefficients

a [AU]	P_2	P_1	P_0
1.3	0.0981	0.9573	0.7566
1.8	0.0960	0.9615	0.7650
2.2	0.0866	0.9763	0.7667

approximation of the $v_{\text{extra}}/v_{\text{orb}}$ value where the angle of impact is zero, in terms of the orbital separation a and mass ratio q as described in equation 2.2.10 and portrayed in figure 2.2.1.

$$\begin{aligned}\frac{v_{extra}}{v_{orb}}(\alpha_{imp}=0)_{3b} =&(-0.0216a^2+0.0629a+0.0530)q^2\\ &+(0.0320a^2-0.0909a+1.0214)q\\ &+(-0.0142a^2+0.0610a+0.7013)\end{aligned} \tag{2.2.10}$$

Any result to the left of this point produces a particle that impacts the accretor in a prograde motion with respect to the binary's orbital motion, while any result to the right impacts the accretor with a retrograde velocity.

The second difference between our results and the three-body approach appears in the range of $v_{\text{extra}}/v_{\text{orb}}$ values where impact occurs. In the case of the three-body approximation, we get a much wider range of values, particularly extending to far greater $v_{\text{extra}}/v_{\text{orb}}$ to the right of $\frac{v_{extra}}{v_{orb}}(\alpha_{imp}=0)_{3b}$. This behaviour is caused by the last term of equation 2.1.1: since our calculation of $L1$ depends on the particle's initial velocity, a donor with a faster rotation rate produces a $L1$ position that sits closer to the accretor star, thus helping direct accretion occur.

The range of $v_{\text{extra}}/v_{\text{orb}}$ values explored in this section (> 0.8) all require the donor's rotation to be supersynchronous to its orbital motion, as seen in figure 2.2.2. Furthermore, the results from the three-body approach require the donor to fully rotate at least twice for each orbital period. The implications of this will be discussed in section 4, however, in this section we will focuss on the lower end of $v_{\text{extra}}/v_{\text{orb}}$ values where each model experiences direct accretion.

By observing the results of both the three-body approach and our model, we can see there is a relation between the minimum $v_{\text{extra}}/v_{\text{orb}}$ for direct accretion, and

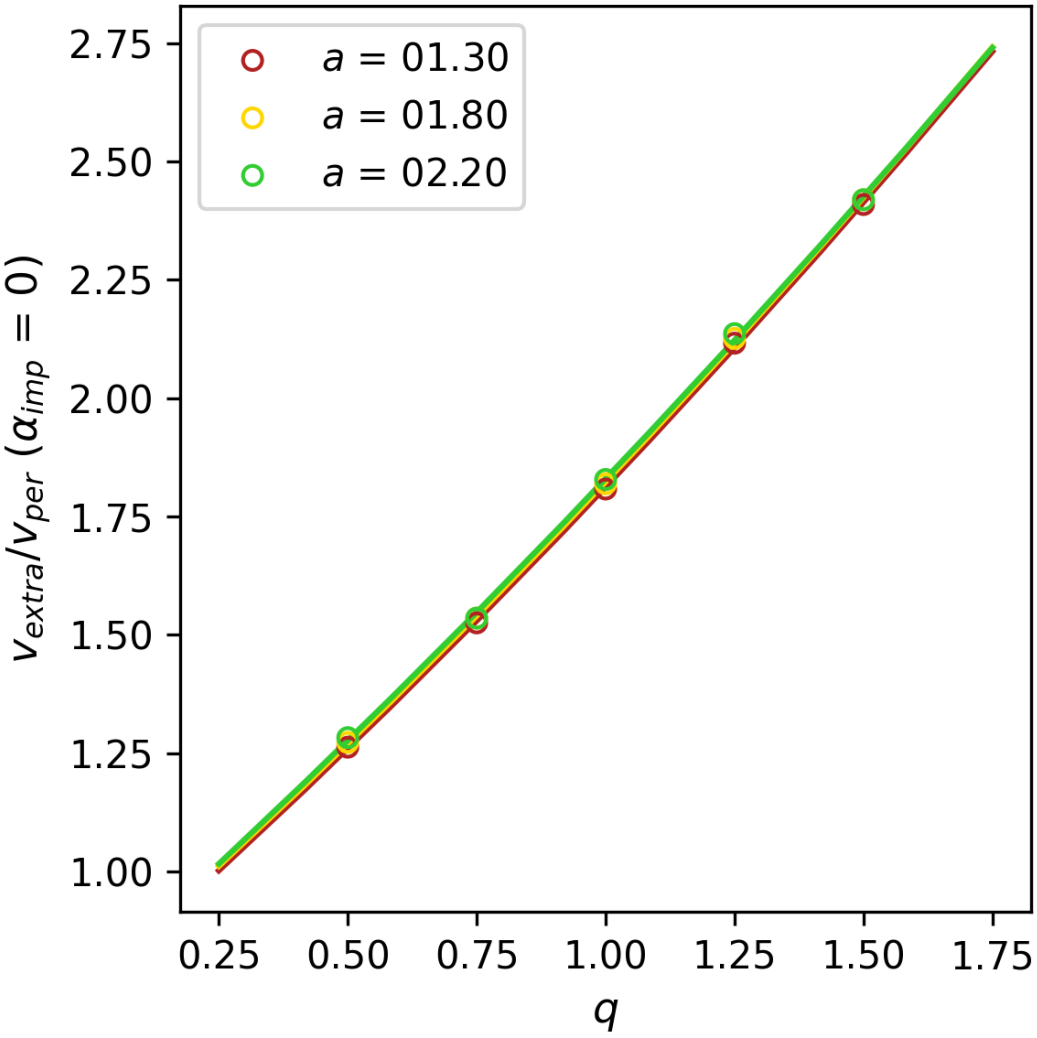

Figure 2.2.1: Value of $v_{\text{extra}}/v_{\text{orb}}$ for which the impact angle α_{imp} becomes 0, as a function of the mass ratio q, for systems with a = 1.30, 1.80 & 2.20 AU (red, yellow and green respectively). The open circles show the resulting value from a three-body approach while the solid lines plot the best fit, described by equation 2.2.10.

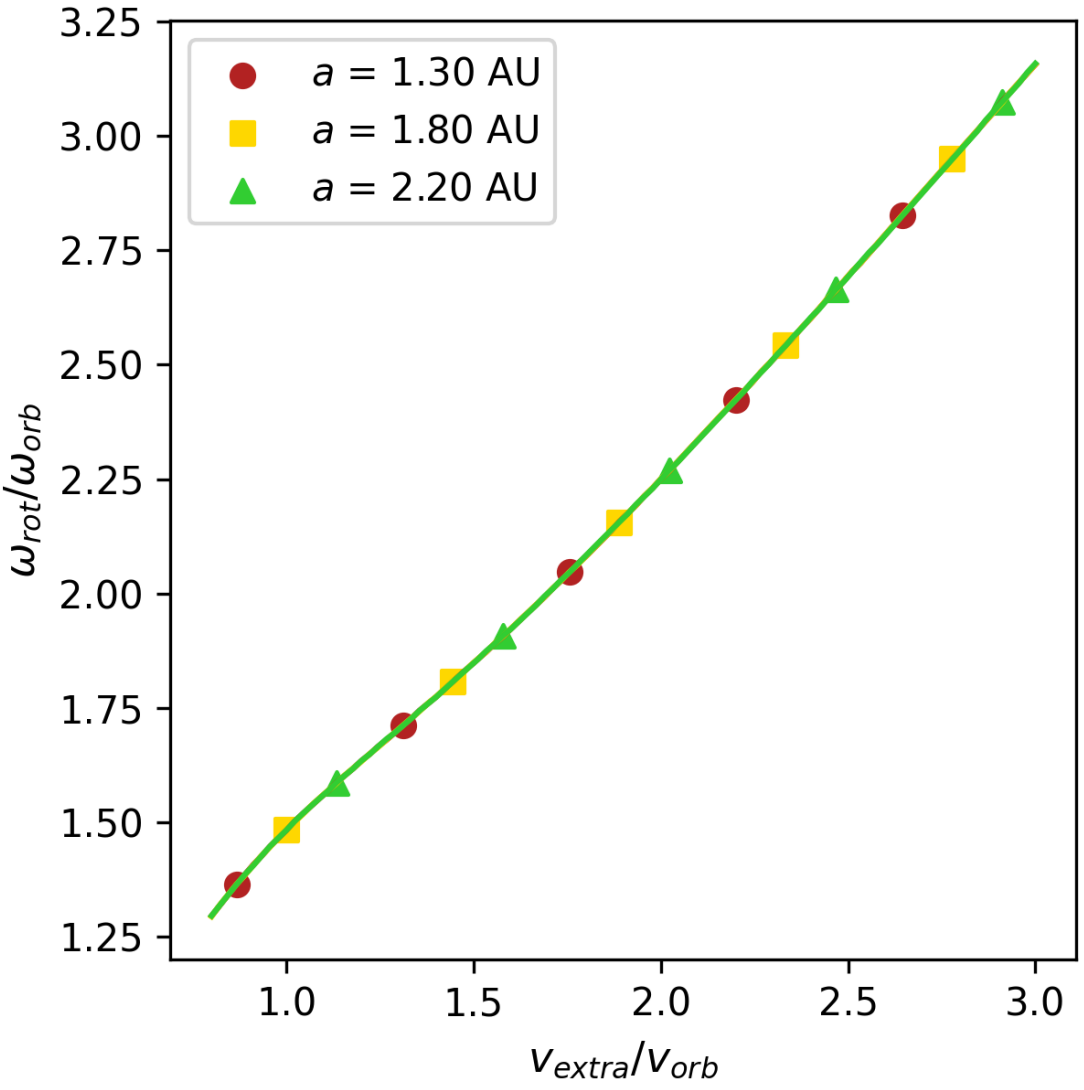

Figure 2.2.2: Angular rotational speed of the donor, in terms of the angular orbital velocity of the binary system, as a function of $v_{\text{extra}}/v_{\text{orb}}$. Here, it is assumed that the donor's radius is equal to $a - r_{L1}$.

the semi-major axis a. We will refer to the difference between $\frac{v_{extra}}{v_{orb}}(\alpha_{imp}=0)_{3b}$ and this minimum value as "amplitude A_{3b}". We too can get an approximation of this amplitude in terms of a and q via polynomial fitting. The expression with the best fit coefficients for the amplitude of the three-body data is

$$\begin{aligned} A_{3b} =&(0.\overline{04}q - 0.\overline{02})a^2 \\ &+ (-0.\overline{18}q + 0.\overline{07})a \\ &+ (0.46\overline{70}q - 0.16\overline{28}) \end{aligned} \tag{2.2.11}$$

This approximation is displayed visually in figure 2.2.3.

Furthermore, the amplitude in our model's results can be approximated as

$$\begin{aligned} A =&(0.0210q^2 - 0.0470q + 0.03\overline{5})a^2 \\ &+ (-0.0695q^2 + 0.1565q + 0.15\overline{2})a \\ &+ (0.0493q^2 - 0.1114q + 0.2508) \end{aligned} \tag{2.2.12}$$

Then, to better approximate our results to the more realistic case of a three-body problem, we can correct our initial $v_{\text{extra}}/v_{\text{orb}}$ values through equation 2.2.13

$$\left(\frac{v_{extra}}{v_{orb}}\right)_{\text{corr}} = \frac{A_{3b}}{A}\left(\frac{v_{extra}}{v_{orb}} - 1\right) + \frac{v_{extra}}{v_{orb}}(\alpha_{imp}=0)_{3b} \tag{2.2.13}$$

The effects of this correcion can be seen in figure 2.2.4.

Although this correction shows that the results of our model can be approximated to those from the planar restricted circular three-body case, having the impact angle equal zero when $v_{\text{extra}}/v_{\text{orb}} = 1$ allows for a more straightforward explanation. Then, for the sake of simplicity, the correction is not applied to any of the results in the subsequent sections.

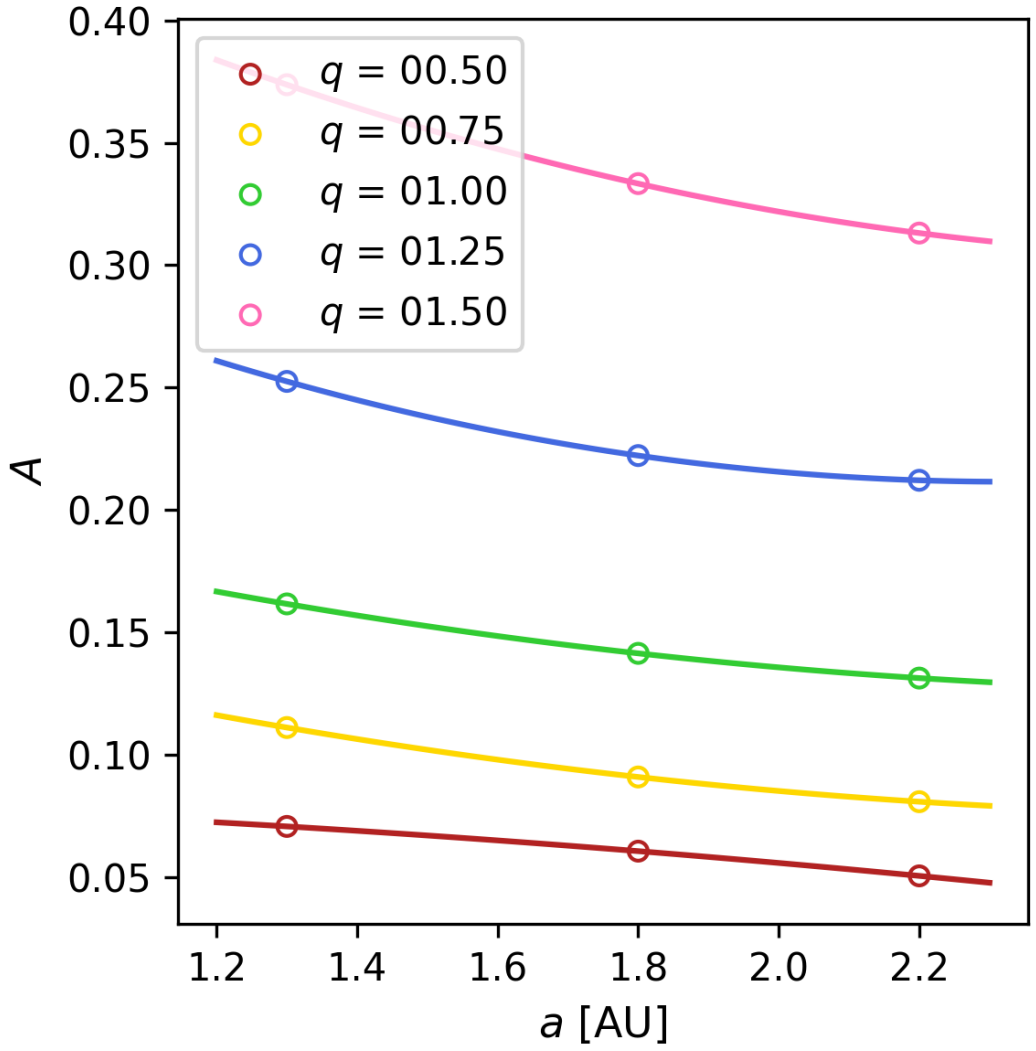

Figure 2.2.3: Amplitude A, as a function of the semi-major axis a, for systems with $q = 0.50,\ 0.75,\ 1.00,\ 1.25$ & 1.50 (red, yellow, green, blue and pink respectively). The open circles show the resulting value from a three-body approach while the solid lines plot the best fit, described by equation 2.2.11.

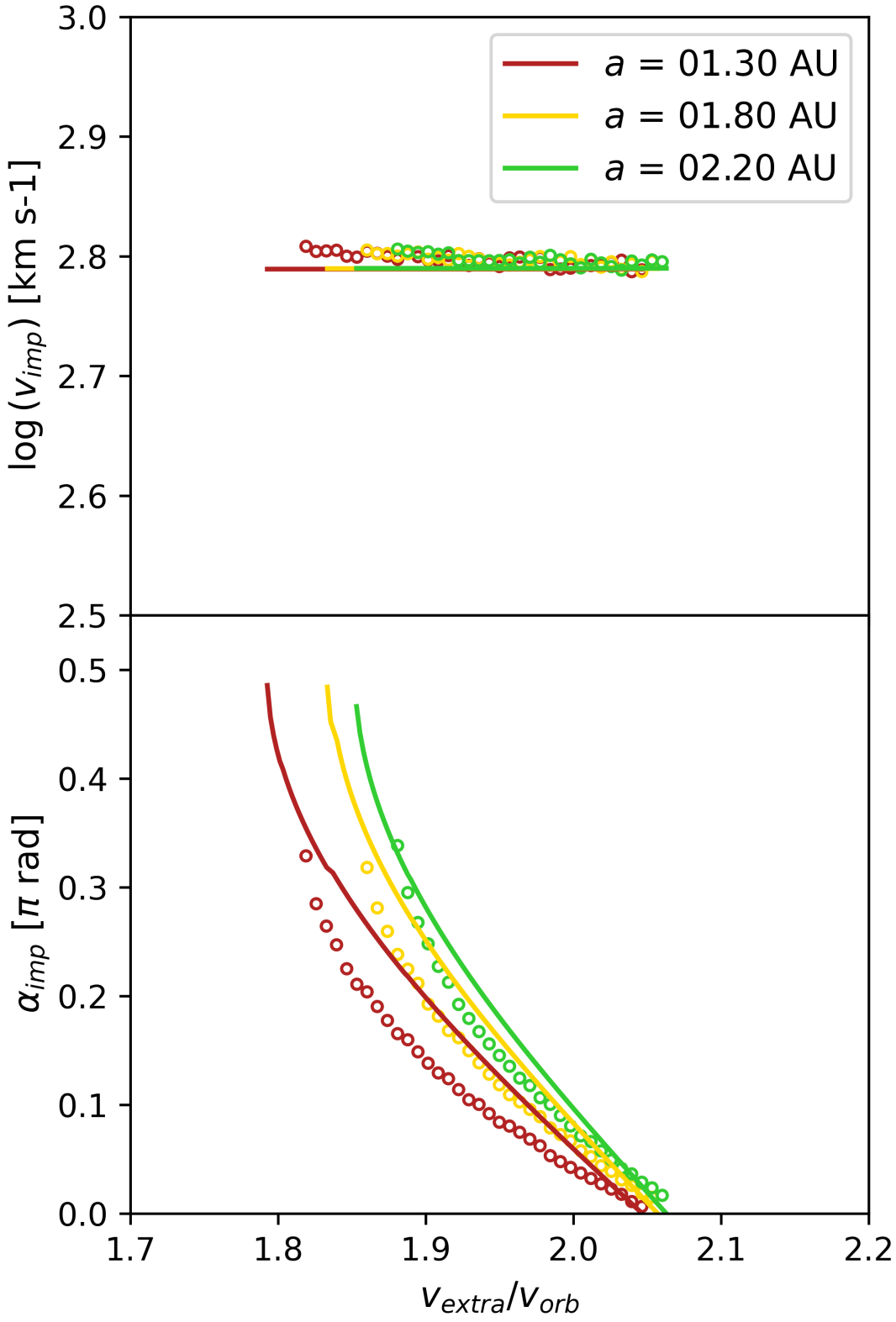

Figure 2.2.4: Impact velocity in a logarithmic scale (top) and angle (bottom) for systems of an orbital separation $a = 1.30$, 1.80 & 2.20 au (red, yellow & green) as a function of v_{extra}/v_{orb}. The data corresponding to our model (solid lines) has been corrected through equation 2.2.13 to better approximate the three-body results (open circles). Only data where $v_{\text{extra}}/v_{\text{orb}} < \frac{v_{extra}}{v_{orb}}(\alpha_{imp} = 0)_{3b}$ is displayed.

Chapter 3

Results

3.1 Spin-up

The spin-up effect suffered by the accretor star after a single orbital period, and how this is influenced by changes in the binary's semi-major axis, eccentricity and the donor's rotation rate, will be analyzed in the following subsections.

3.1.1 Semi-major axis a

In the simplest case of a circular orbit (e.g. red curve on the left panel of figure 3.1.1), the spin-up provided by the accreted mass over a single period is greater for larger values of a. A larger orbital separation means that each parcel will drop from a greater distance, building up speed and impacting the accretor with higher velocities. In addition, the impact point drifts away from the line connecting the center-of-mass of the accretor to the center-of-mass of the donor, arriving closer to the edge and maximizing the tangential component, therefore providing a greater amount of angular momentum to spin the star up.

A system with $v_{\text{extra}}/v_{\text{per}} = 0.90$, $e = 0.00$, $m_{\text{acc}} = 1M_{\odot}$ and $m_{\text{don}} = 1.2M_{\odot}$ is the most effective at spinning up its accretor when $a = 1.86$ AU. For this value of a, the parcel dropped from the orbit's periapsis impacts the accretor completely tangentially, thus maximizing the spin-up provided by it. In the general case, the a value for the peak in spin-up can be obtained by following a similar analysis to that of Appendix A1. Having a fixed value for v_i, equations A1.6 and A1.9 can be rearranged into a new expression for the semi-major axis value at which the

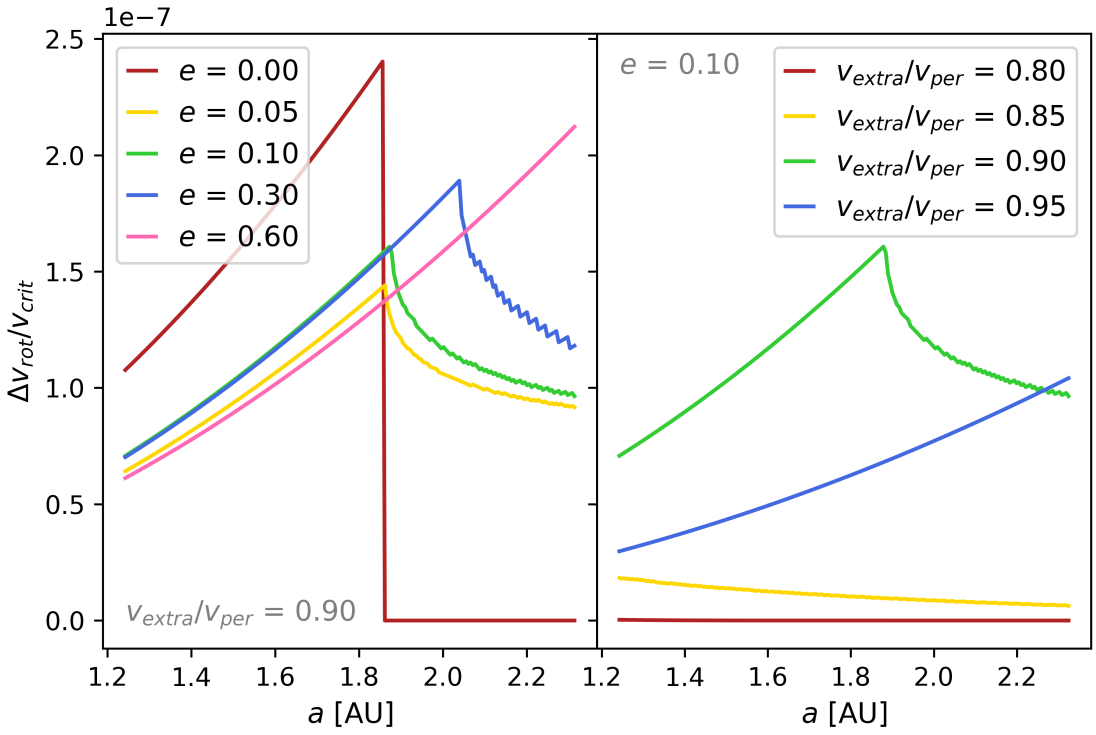

Figure 3.1.1: Spin-up of the accretor star in terms of its critical rotational velocity after one orbital period, as a function of the binary system's semi-major axis a. Left: All systems have $v_{\rm extra}/v_{\rm per} = 0.90$ and e takes the values 0.00, 0.05, 0.10, 0.30 & 0.60, shown by different colors (red, yellow, green, blue and pink). Right: All systems have $e = 0.1$ and $v_{\rm extra}/v_{\rm per}$ takes the values 0.80, 0.85, 0.90, & 0.95 (red, yellow, green and blue).

peak in spin-up occurs

$$a_{peak} = \frac{1+e}{1-e}\left(r_{L1} + \frac{r_{L1}^2}{r_{\rm acc}}\right)\left(1 - \frac{v_{\rm extra}}{v_{\rm per}}\right)^2\left(\frac{m_{\rm acc}+m_{\rm don}}{2m_{\rm acc}}\right) \tag{3.1.1}$$

By replacing this into equation 2.1.1 for $r = r_{\rm per} = a(1-e)$, r_{L1} can be obtained numerically and replaced back into equation 3.1.1. The results are shown in figure 3.1.2.

On the left panel $a_{\rm peak}$ is graphed as a function of e. The semi-major axis value at wich the peak in spinup occurs grows with eccentricity, showing a clear asymptote at $e = 1.0$.On the right panel, $a_{\rm peak}$ is shown as a function of $v_{\rm extra}/v_{\rm per}$ instead. Within our a range, a_{peak} seems very sensitive to small changes in the donor's rotational velocity, when compared to the more gradual growth portrayed in the left panel. As $v_{\rm extra}/v_{\rm per}$ approaches 1, the initial velocity of the parcel at periastron gets closer to $v_i = 0$, making the centripetal force term in equation

2.1.1 negligible, this means the parcel's impact on the accretor's surface will be almost entirely radial and the spin-up provided by it will solely depend on the impact speed which is maximized by increasing the initial distance from which the parcel falls.

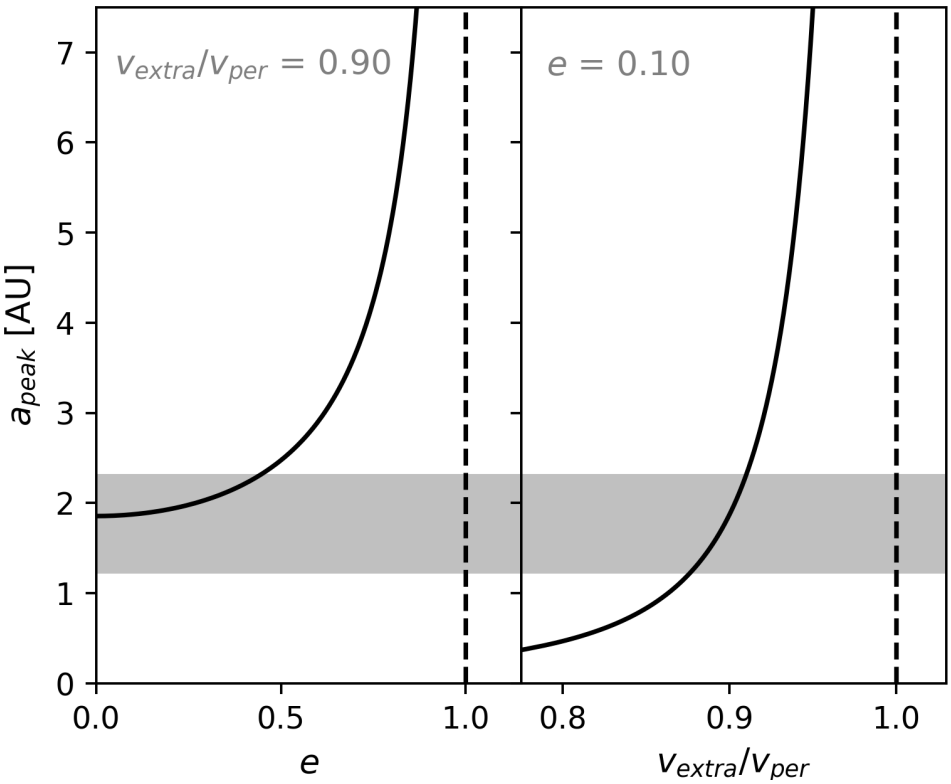

Figure 3.1.2: Semi-major axis value for maximum spin-up of the accreting star as a function of the system's eccentricity with constant $v_{\text{extra}}/v_{\text{per}} = 0.90$ (left) and the donor's rotation with constant $e = 0.10$ (right). The shaded region marks the range of a we work with in the analysis.

For larger a than that of the critical point, condition 2 fails to be fulfilled at periastron, producing a drop in spin-up. A parcel at periastron will miss the edge of the accreting star and fail to directly impact its surface. This means that, for a circular orbit, accretion will completely cease for a larger than that of the peak while for eccentric systems the region of the orbit where direct impact occurs shrinks away from the major axis, detaching from periapsis.

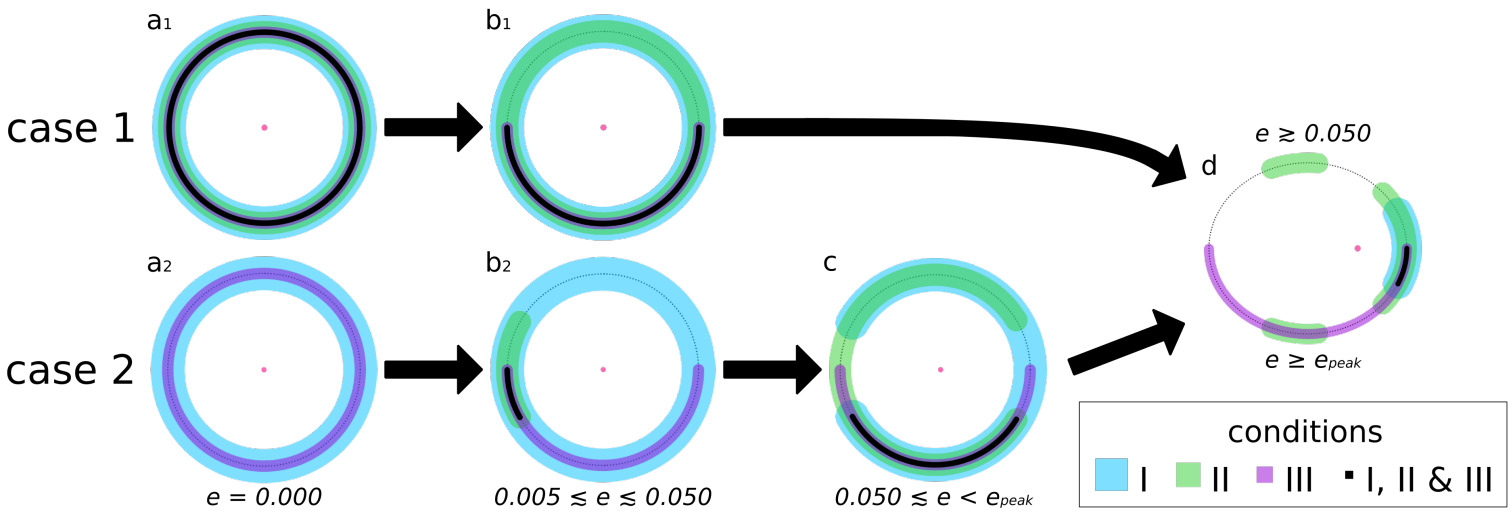

Figure 3.1.3: Graphic representation of cases 1 and 2, of the eccentricity spin-up analysis. The accretor star is depicted by a pink circle whose size has been scaled by a factor of 10. A dotted line draws the orbit of the donor's center of mass and, from widest to narrower, the blue, green and purple regions represent areas of the orbit where conditions 1, 2 and 3 are met, respectively, while the black region represents the intersection of all three. Case 1 is exemplified by the yellow curve ($a = 1.80$ AU) on the left panel of figure 3.1.4, and goes contains stages a_1, b_1 and d for increasing eccentricities. Case 2 is exemplified by the green curve ($a = 2.20$ AU) on the left panel of figure 3.1.4, and goes contains stages a_2, b_2, c and d for increasing eccentricities.

3.1.2 Eccentricity e

As e approaches 1, the spatial resolution at periastron decreases if we choose data points separated by a constant time step dt. This can induce resolution related errors to the calculation of the angular momentum provided in the vicinity of periapsis. We can solve this issue by choosing data points along the orbit that are separated by a constant $d\theta$ instead of setting a constant time step between them. This results in a distribution that does not follow Kepler's law but provides a better resolution for orbits where accretion occurs mostly at periastron. We adhere to our chosen value of 1k data-points per orbit. Increasing this number does not change the results.

In contrast to the previous section, the spin-up curves in figure 3.1.4 follow one of two different trends. A visual depiction of both cases is displayed on figure 3.1.3.

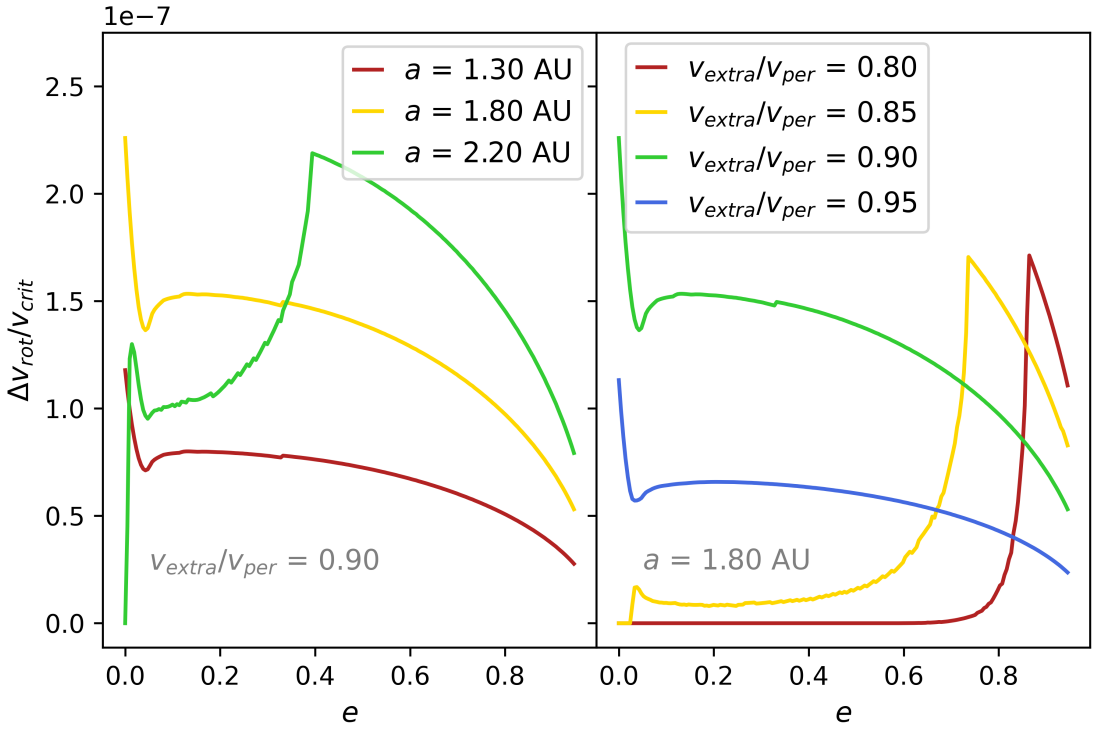

Figure 3.1.4: Spin-up of the accretor star in terms of its critical rotational velocity, as a function of the binary system's eccentricity e. Left: All systems have $v_{\rm extra}/v_{\rm per} = 0.90$. The result is displayed for $a = 1.30$, 1.80 & 2.20 AU (red, yellow and green). Right: All systems have $a = 1.80$ AU and $v_{\rm extra}/v_{\rm per}$ takes the values 0.80, 0.85, 0.90, & 0.95 (red, yellow, green and blue).

The first case (from now on, case 1) follows the pattern shown by the yellow curve in the left panel of figure 3.1.4, where $a = 1.80$ AU. At $e = 0.0$, all three conditions

are satisfied over the entire orbit. For any value greater than 0.0, condition 3 reduces the effective accretion area to the latter half of the orbit (i.e. from past apoastron to periastron), causing the drop in spin-up seen immediately after $e = 0.0$. As e increases, the orbital velocity of the donor at apoapsis decreases and, in consequence, so does the initial velocity of a parcel dropped from there. A smaller v_i in turn causes the parcel to fall to the accretor on a more eccentric orbit, impacting its surface in a primarily radial direction and reducing the amount of angular momentum transferred. This, in addition to f being smaller at apoastron than periastron, minimizes the overall spin-up provided, resulting in the small decline observed towards $e \sim 0.05$. For greater e the region of the orbit where direct accretion occurs shrinks around periapsis while at the same time the impact angle of the parcel decreases, producing the gradual decline observed to the right side of the curve.

The second case (from now on, case 2) is well exemplified by the curve for $a = 2.20$ AU (green) in the left panel of figure 3.1.4, which we will be using for this case's analysis. These spin-up curves do not show a single peak but instead two local critical points. Condition 2 is not met anywhere when the orbit is circular, which is coherent with the results shown on the left panel of figure 3.1.1, and thus no spin-up is provided when $e = 0.00$. For $e > 0.00$, but still close to 0.00, all three conditions for direct accretion are satisfied in a reduced region after apoastron passage and as e increases, the effective area for direct accretion extends from apoastron towards periastron. This expansion of the effective accretion area is however countered by the decline in angular momentum provided from apoastron discussed on case 1's analysys around $e \sim 0.05$, producing a similar drop in spin-up at the same eccentricity. Beyond $e \sim 0.05$ the region where the donor overfills its Roche lobe shrinks, detaching from apoapsis and producing a small drop in spin-up. The combination of this and the expansion of the effective area of condition 2 towards periastron, result in the behaviour seen between eccentricities 0.05 and 0.4. At $e \sim 0.4$ the effective area for direct accretion reaches periastron, producing the main feature of this curve. From this point to higher eccentricities, the region where condition 1 is fulfilled continues to narrow around $\theta = 0$ and the accretion at periapsis becomes more radial, providing less angular momentum to the accretor.

It is worth mentioning that case 1 and case 2 correspond to systems with initial

conditions to the left and to the right of the a_{peak} of figure 3.1.1, respectively.

3.1.3 Donor's rotation

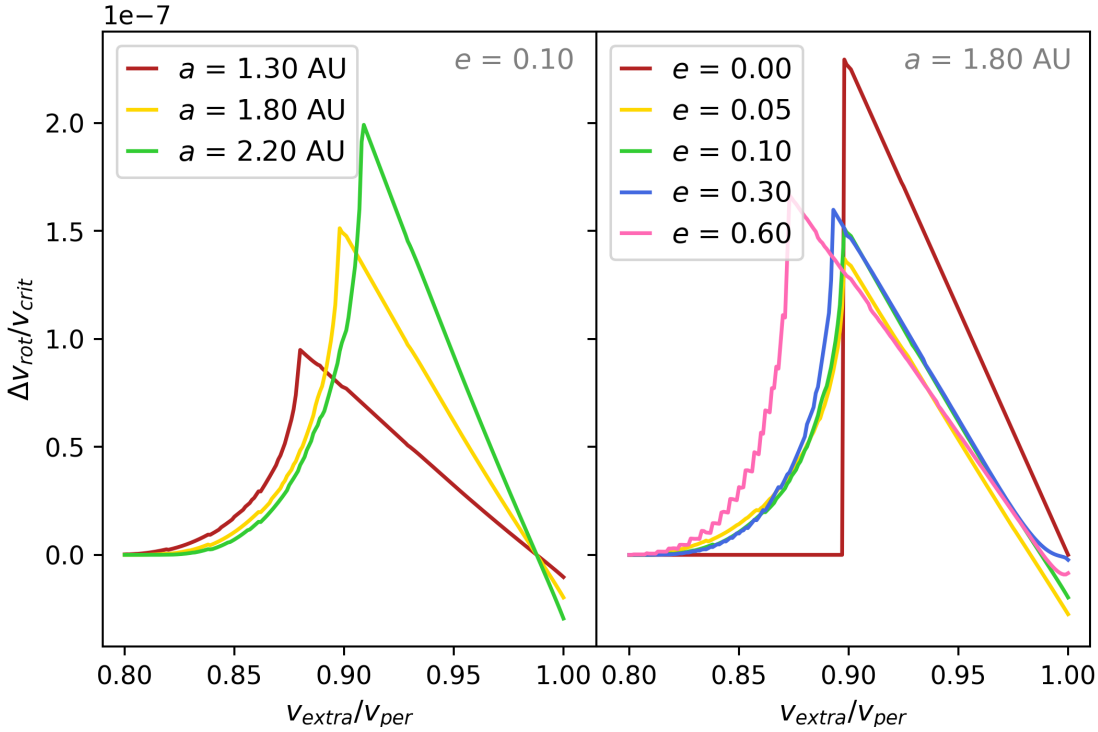

Figure 3.1.5: Spin-up of the accretor star in terms of its critical rotational velocity, as a function of the donor's rotational velocity $v_{\text{extra}}/v_{\text{per}}$. Left: All systems have $e = 0.10$. The result is displayed for $a = 1.30$, 1.80 & 2.20 AU (red, yellow and green). Right: All systems have $a = 1.80$ AU and e takes the values 0.00, 0.05, 0.10, 0.30, & 0.60 (red, yellow, green, blue and pink).

In the case of a circular orbit (red curve on right panel of figure 3.1.5) direct impact occurs only for $v_{\text{extra}}/v_{\text{per}} \gtrsim 0.90$. This mirrors the behaviour observed in the analysis of the circular case in section 3.1.1. Here, the lowest $v_{\text{extra}}/v_{\text{per}}$ value where direct accretion occurs provides the most spin-up to the accreting star.

Higher prograde rotation velocities produce more eccentric trajectories for the parcels of mass, impacting the accretor in a mostly radial direction and therefore minimizing the transferred angular momentum.

This behaviour is consistent for non-circular orbits, with the difference of a gradual increase towards the peak instead of the abrupt rise in spin-up.

At the lowest value of $v_{\text{extra}}/v_{\text{per}}$ where spin-up is non-zero, only a small region of

the orbit produces direct accretion. Within the region were the donor overfills its Roche lobe, only the section that is farthest from periastron meets condition 2.

An increase in $v_{\text{extra}}/v_{\text{per}}$ extends this region towards periapsis where the peak in spin-up is reached.

3.2 Conservativeness

We compute how conservative a system is by comparing the mass the donor looses dm_{don} with the mass that directly impacts the accretor dm_{acc} in one orbital period.

Within the orbit, the donor star sheds mass from its envelope where both condition 1 & condition 3 are met simultaneously, while the accretor gains mass only when all three conditions are met. Under this premise, a fully conservative system is such that all mass leaving the donor directly impacts the accretor's surface. Even if the parcels that miss the accretor might be able to continue orbiting the star and form a disk, they will not be counted as gained mass on the accretor side for this analysis.

Any system where $|dm_{\text{acc}}/dm_{\text{don}}| < 1$ has a region in the orbit where the mass parcels lost by the donor are not directly accreted by the companion. If these parcels were to continue orbiting the accretor, a disk could be formed. Depending on the density of this disk in comparison to the parcels whose velocities produce direct impact, its presence could prevent further direct accretion from occurring in a subsequent passage of the donor. Further discussion on the consequences of disk formation regarding the angular momentum transfer to the accretor will be discussed in a later section.

3.2.1 Semi-major axis a

The conservativeness of these systems reflects the behaviour seen in the spin-up curves in section 3.1.1. By comparing those results with figure 3.2.1, we see that the systems with a values lower than that of the peak in spin-up are completely conservative while those with $a > a_{\text{peak}}$ present a decline in $|dm_{\text{acc}}/dm_{\text{don}}|$ due to condition 2 forcing the accretion effective area to shrink away from periapsis.

The fully conservative nature of systems with $a \leq a_{\text{peak}}$ make them the most effective at direct accretion. The fact that all the mass lost by the donor is gained

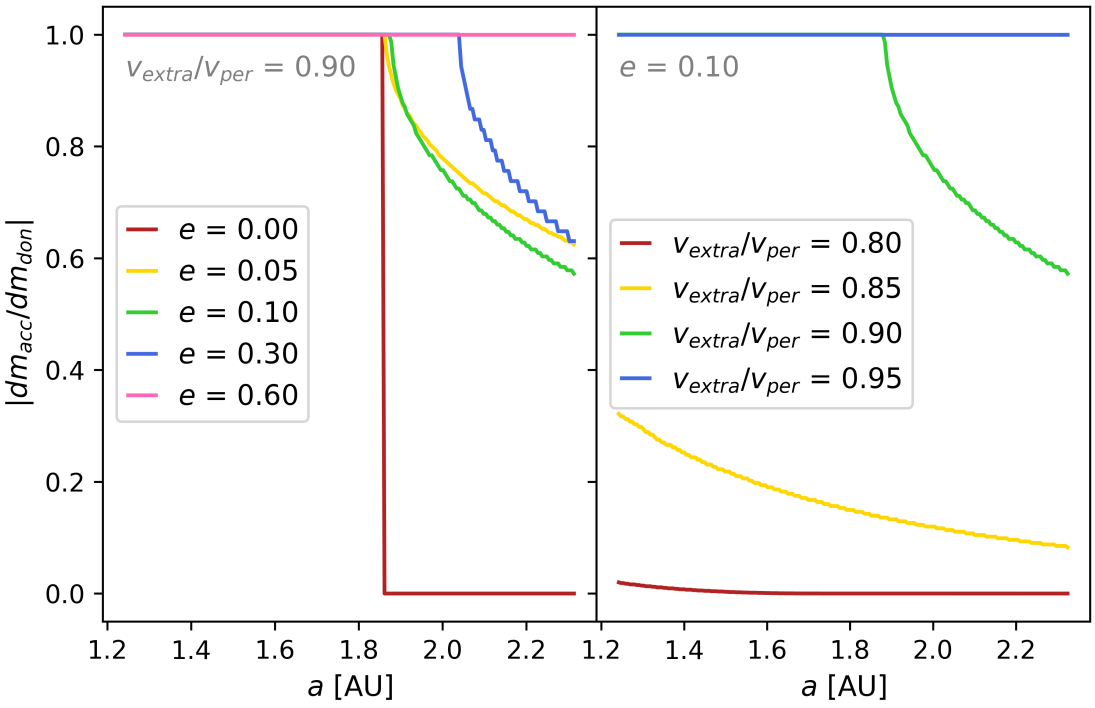

Figure 3.2.1: Conservativeness of the accretion event, as a function of the binary system's semi-major axis a. Left: All systems have $v_{\text{extra}}/v_{\text{per}} = 0.90$. The result is displayed for $e = 0.00$, 0.05, 0.10, 0.30 & 0.60 (red, yellow, green, blue and pink). Right: All systems have $e = 0.10$ and $v_{\text{extra}}/v_{\text{per}}$ takes the values 0.80, 0.85, 0.90 & 0.95 (red, yellow, green and blue).

by the accretor through direct accretion means there is no chance for a disk to form. Systems with $a > a_{\text{peak}}$, however, have a region close to periapsis where the donor's lost mass is not directly accreted.

3.2.2 Eccentricity e

In section 3.1.2 the resulting spin-up curves were divided into two cases. First, those that had $\Delta v_{\text{rot}}/v_{\text{crit}} > 0$ in a circular orbit and appeared smooth (i.e. yellow in left panel and green and blue in the right panel of figure 3.1.4). Second, those with $\Delta v_{\text{rot}}/v_{\text{crit}} = 0$ at $e = 0$ and a noticeable peak somewhere in the distribution (i.e. green in the left panel and red and yellow in the right panel of figure 3.1.4). We will refer to systems whose spin-up curves resemble these regimes as case 1 and case 2 respectively.

Systems within case 1 are conservative through the whole range of e values as observed in the left panel of figure 3.2.2 by curves for $a = 1.30$ AU & $a = 1.80$

AU, and curves for $v_{\text{extra}}/v_{\text{per}} = 0.90$ & $v_{\text{extra}}/v_{\text{per}} = 0.95$ on the right panel of the same figure.

We will use the curve for $a = 2.20$ AU (green) in the left panel of figure 3.2.2 to analyze case 2 systems. The shape of this system's conservativeness curve is consistent with the behaviour explored in the spin-up section for these same systems. None of the shed mass is directly accreted on a circular orbit due to condition 2 failing to be met anywhere in the orbit. Condition 2 is first fulfilled at apoapsis for very small e and extends its domain towards periapsis as e increases, nonetheless, at $e \sim 0.05$ the donor is unable to fill its Roche lobe at the orbit's apoastron, making the region where condition 1 recede around periastron. The combination of these two factors is responsible for the shape of the curve at $0.00 < e \lesssim 0.4$. Around $e \sim 0.4$, the region of the orbit where a parcel's orbit would intersect the accretor reaches periapsis, intersecting the domain of condition 1 in its entirety.

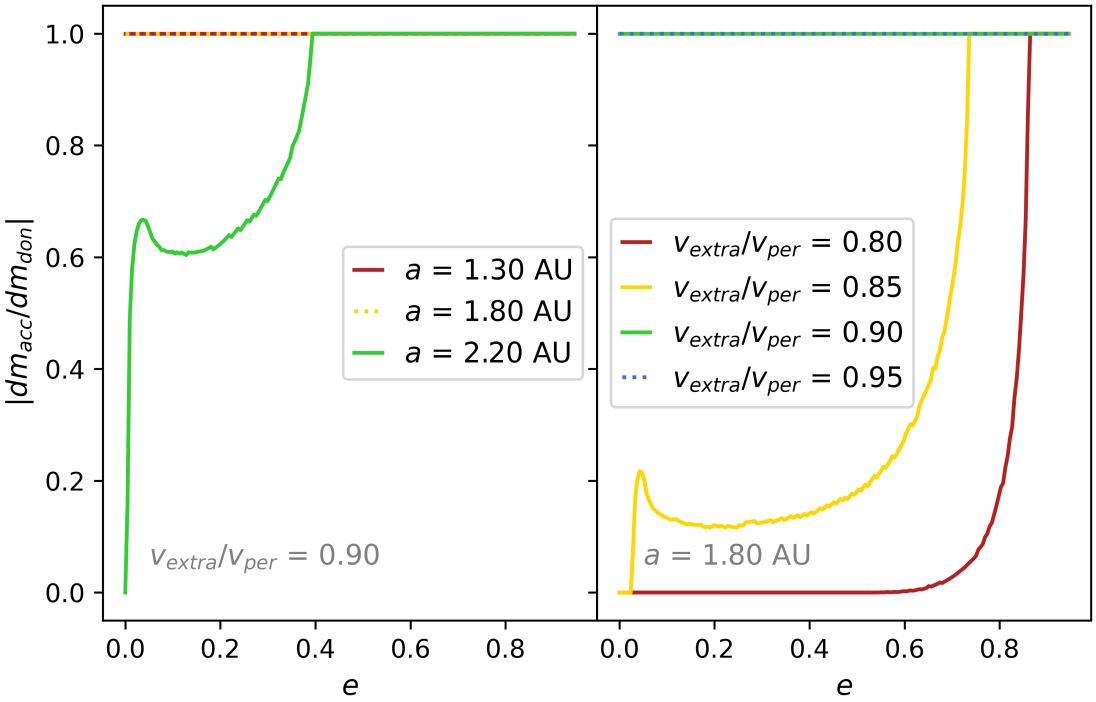

Figure 3.2.2: Conservativeness of the accretion event, as a function of the binary system's eccentricity e. Left: All systems have $v_{\text{extra}}/v_{\text{per}} = 0.90$. The result is displayed for $a = 1.30$, 1.80 & 2.20 AU (red, yellow and green). Right: All systems have $a = 1.80$ AU and $v_{\text{extra}}/v_{\text{per}}$ takes the values 0.80, 0.85, 0.90, & 0.95 (red, yellow, green and blue).

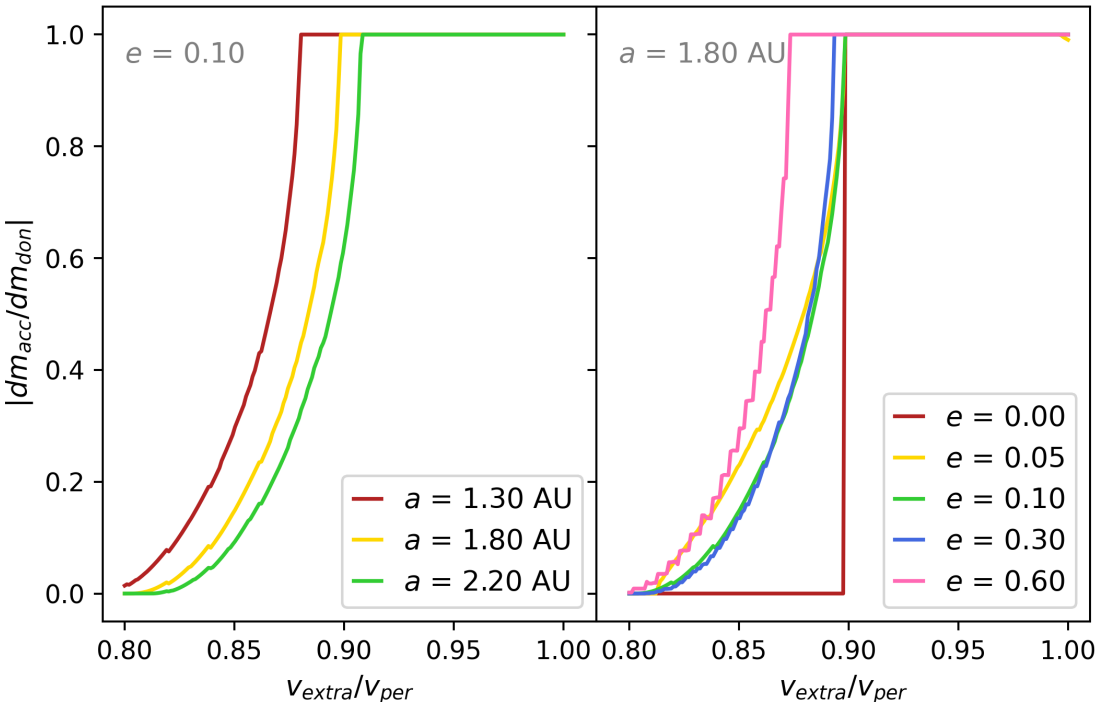

Figure 3.2.3: Conservativeness of the accretion event, as a function of the donor's rotational velocity $v_{\rm extra}/v_{\rm per}$. Left: All systems have $e = 0.10$. The result is displayed for $a = 1.30$, 1.80 & 2.20 AU (red, yellow and green). Right: All systems have $a = 1.80$ AU and e takes the values 0.00, 0.05, 0.10, 0.30, & 0.60 (red, yellow, green, blue and pink).

3.2.3 Donor's rotation

For all cases displayed in figure 3.2.3, conservativeness increases with $v_{\rm extra}/v_{\rm per}$ until reaching unity at the same donor rotation value where the peak in spin-up is achieved.

All systems with a donor rotation rate lower than the velocity of the peak cause their donor to loose mass around periastron that fails to impact the accretor.

3.3 Mass ratio q

Figure 3.3.1 shows the spin-up dependence on a for different mass ratios $q = m_{\rm don}/m_{\rm acc}$. The accretor mass $m_{\rm acc} = 1 M_\odot$ was kept constant. We can see that, when comparing with figure 3.1.1, the overall behaviour of the curve is the same, but the position of the peak and its maximum spin-up value change with q.

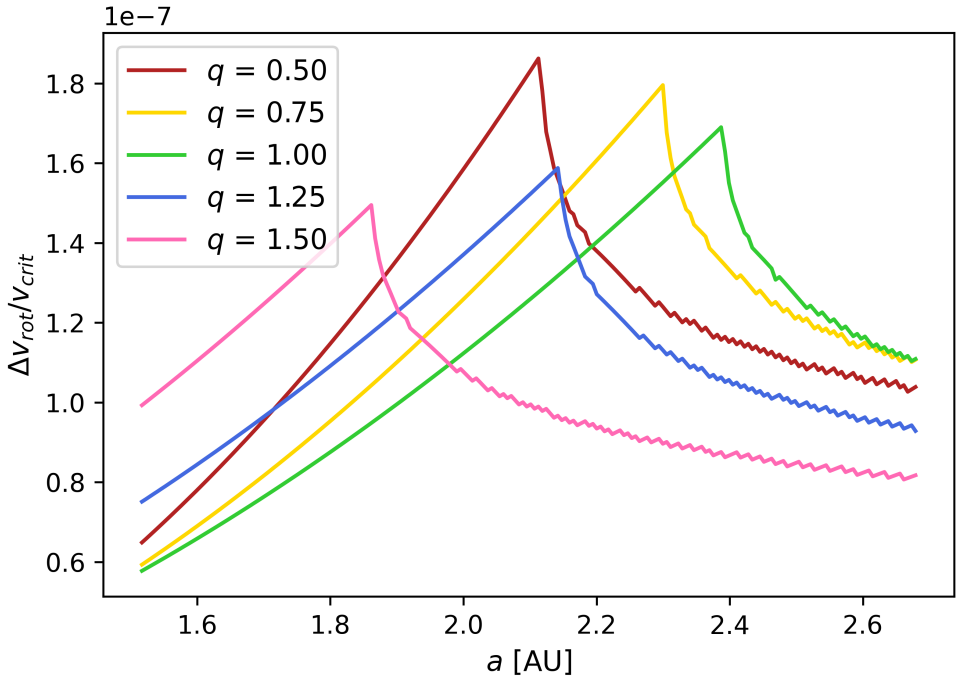

Figure 3.3.1: Alike figure 3.1.1 but for $q = 0.50$, 0.75, 1.00, 1.25 & 1.50 and constant $e = 0.10$ and $v_{\text{extra}}/v_{\text{per}} = 0.90$.

The value of a_{peak} reaches its maximum value when the donor and accretor have the same mass and shifts towards smaller a for both $q < 1$ and $q > 1$. Equation 2.1.1 is dependent on the masses of both stars, therefore a change in the mass ratio also changes the starting point of a particle r_{L1}.

The maximum spin-up for all q values is still of the order of 10^{-7}, however there is a subtle increase related to a decrease in q. For a donor mass of $m_{\text{don}} = 1.5M_{\odot}$ the maximum spin-up is $\sim 1.5 \times 10^{-7} v_{\text{crit}}$ while a donor mass of $m_{\text{don}} = 0.5M_{\odot}$ results in a spin-up of $\sim 1.9 \times 10^{-7} v_{\text{crit}}$. Althought a $\sim 4 \times 10^{-8} v_{\text{crit}}$ might seem small, it is not negligible when compared with a spin-up effect of the order of $10^{-7} v_{\text{crit}}$. In future work, a wider exploration of the parameter space in regards to q would help us understand more extreme cases. Nevertheless, we note that our model can propperly account for different mass ratios.

3.4 Timescale

A spin-up of the order of $10^{-7} v_{\text{crit}}$ per period implies that, if the orbital parameters of the binary and the mass loss ratio of the donor stay invariant, it would take

$\sim 10^7$ periods (9.20 to 23.53 Myr for 1.23 AU $< a <$ 2.30 AU) for the accretor to reach critical rotation. Yet, assuming our donor has a $0.53 M_\odot$ core and $\dot{M} = 10^{-6} M_\odot/\mathrm{yr}$, it would only take 0.67 Myr to completely shed its envelope.

3.5 L1

Equation 2.1.1 differs from the usual prescription of the $L1$ point by adding a component to account for the centripetal force acting on the parcel, given its initial velocity. This inclusion moves the starting point of the particle closer to the accretor with respect to the actual $L1$ point.

In contrast to figure 2.2.2, figure 3.5.1 shows the relation between $v_{\mathrm{extra}}/v_{\mathrm{orb}}$ and the donor's rotational angular velocity if we remove the centripetal force from the computation of $L1$. Under this prescription, the required donor's rotational angular velocity to produce direct accretion is ~ 1.5, only slightly greater than the ~ 1.25 value found previously. However, $\omega_{\mathrm{rot}}/\omega_{\mathrm{orb}}$ seems to be more sensitive to a change in - when removing the centripetal term, almost doubling ($\omega_{\mathrm{rot}}/\omega_{\mathrm{orb}} \sim 6$) our previous result ($\omega_{\mathrm{rot}}/\omega_{\mathrm{orb}} \sim 3$) for $v_{\mathrm{extra}}/v_{\mathrm{orb}} = 3$.

Although the choice to include a centripetal term into our initial position calculation does not change the fact that supersynchronization is necessary for direct accretion to occur, greater $\omega_{\mathrm{rot}}/\omega_{\mathrm{orb}}$ values imply a greater deviation from equillibrium (corotation). Althought an in-depth analysis of the different effects these initial conditions have will improve this model, it is out of the scope of this investigation and it is left to be explored in future work.

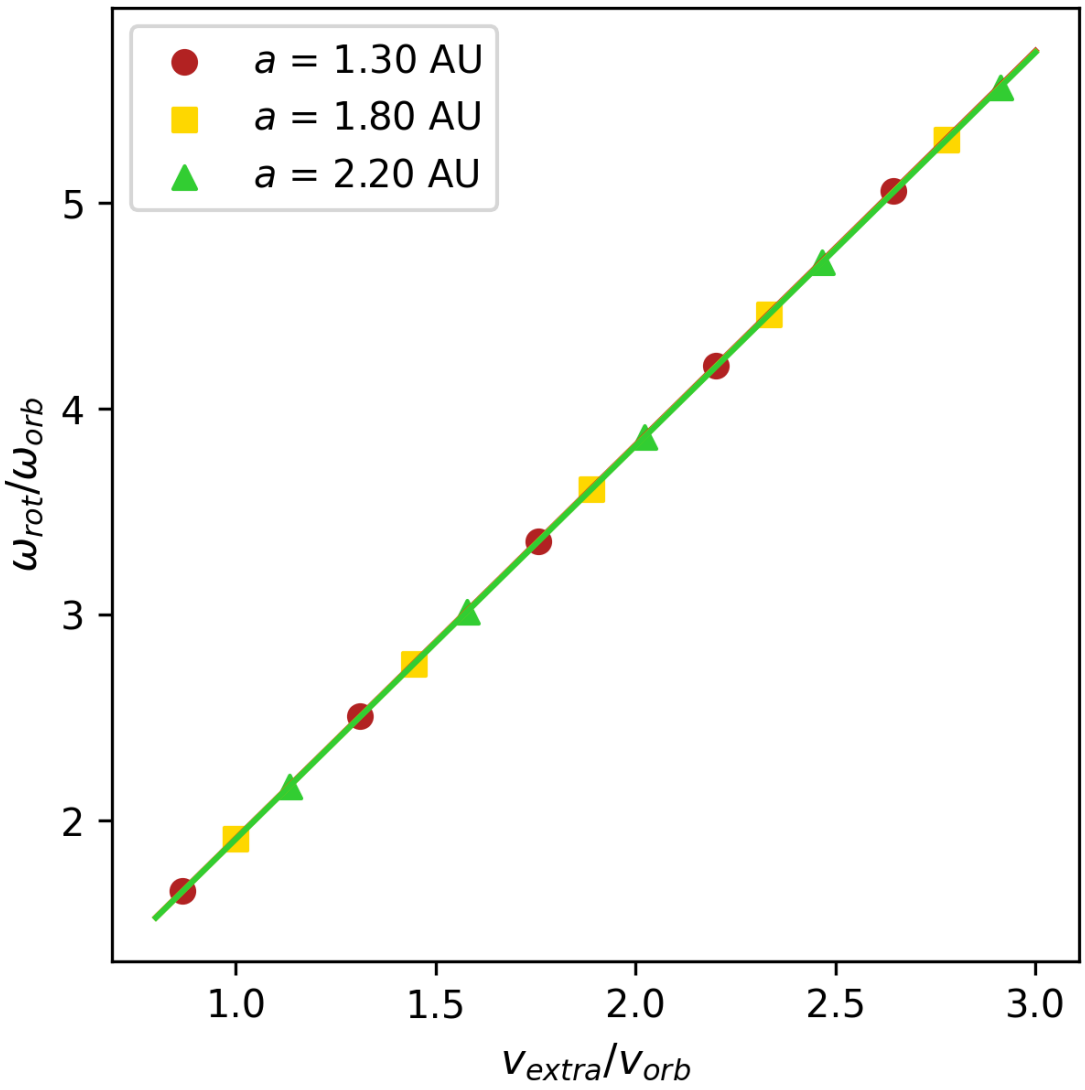

Figure 3.5.1: Akin to figure 2.2.2 except here the $L1$ calculation does not include the term for centripetal force.

Chapter 4

Discussion

4.1 Synchronization

As briefely mentioned in section 2.2 when comparing the circular case in our model to a planar restricted three-body approach, the minimum $v_{\text{extra}}/v_{\text{orb}}$ value needed to get a direct accretion event corresponded to a supersynchronous regime in both our model ($\omega_{\text{rot}}/\omega_{\text{orb}} \sim 1.3$) and the three-body model ($\omega_{\text{rot}}/\omega_{\text{orb}} \sim 2.2$). Supersynchronization deviates from the expected equilibrium state of corotation

For circular orbits, equation 33 of Moreno et al. (2011) expresses the synchronization time

$$\tau_{\text{syn}} = \frac{I(\beta_0^2)\omega_{\text{orb}}^2}{2\dot{E}}$$

where I is the moment of inertia and $\dot{E}$ the rate of energy dissipation. This timescale is dependant on the system's orbital separation "a" and the proportion of a star's rotation to the system's angular orbital velocity "β_0" (i.e. how synchronous the rotation is to the orbit, or $\omega_{\text{rot}}/\omega_{\text{orb}}$). A smaller β_0 results in a longer time, meaning that systems with faster rotating donors would synchronize quicker than those that start closer to equilibrium. From figure 7 of their work, circular systems with a mass ratio $q = 1.25$ ($m_{acc} = 4M_\odot$ and $m_{don} = 5M_\odot$), an orbital separation $a = 0.30$ AU ($\log(a/R_\odot) = 1.8$) and $v_{\text{extra}}/v_{\text{orb}} = 0.73$ & 1.70 ($\beta_0 = 1.2$ & 2.0 respectively) would have synchronization times of 100 Gyr and 25.12 Gyr respectively. It is important to note that the synchronization time is proportional

to a^6, and since the minimum orbital separation value we explore ($a \sim 1.25$ AU) is greater than the maximum value shown in figure 7 from Moreno et al. (2011), we expect the synchronization times for our parameter space to be even greater.

From the work of Counselman (1973) on tidal evolution and the stability of a two-body system upon perturbations, Hut (1980) found that the unique state of equilibrium (coplanar, circular, corotating) is only stable when the ratio between orbital and rotational angular momentum is greater than 3. Figure 4.1.1 shows the orbital to rotational angular momentum ratio α in contrast to our parameter $v_{\text{extra}}/v_{\text{per}}$. In Hut (1981), systems for which the equilibrium state is stable are divided in three cases: (i) If $\alpha - 3 <\ll 1$ it takes the system a longer time to achieve synchronization, (ii) if α is of the order of 7 synchronization and changes in other parameters happen at similar timescales, and (iii) if $\alpha \gg 7$ the system tries to synchronize quickly but since the timescale for circularization of the orbit is much greater, the system enters a state of pseudo-synchronicity. For elliptical orbits, Hut (1981) describes pseudo-synchronization as a state where rotation and orbital motion are near synchronous at periastron ($0.8 < \omega_{\text{rot}}/\omega_{\text{per}} \leq 1$). Pseudo-synchronization deviates from the unique equilibrium state since it forces the rotational period of the star to remain shorter than that of the orbit.

In figure 4.1.1 we can see that for $v_{\text{extra}}/v_{\text{per}} < 1$, all systems fall above the $\alpha = 3$ limit for stability at equillibrium. If we consider the three cases presented by Hut (1981), we could expect a system with an eccentricity of $e = 0.60$ to pseudo-synchronize quicker than systems with lower eccentricities. Figure 4.1.2 shows a clearer comparison between parameter $v_{\text{extra}}/v_{\text{per}}$ and synchronicity at periastron. From there, bear in mind that at the minimum value of $v_{\text{extra}}/v_{\text{per}}$ to achieve direct accretion ($v_{\text{extra}}/v_{\text{per}} \gtrsim 0.80$), the donor's rotational angular velocity must be greater than the instant orbital angular velocity at periastron. In spite of that, we note that there is no need for the whole star to be spining at such rates but rather its outermost layers only. This could be achieved by the tides affecting the surface, nevertheless, further discussion about the mechanisms by which these rotational velocities could be obtained and mantained by the donor star are not part of this work, but will be included in future research.

Moreno et al. (2011) also found timescales for pseudo-synchronization in the case

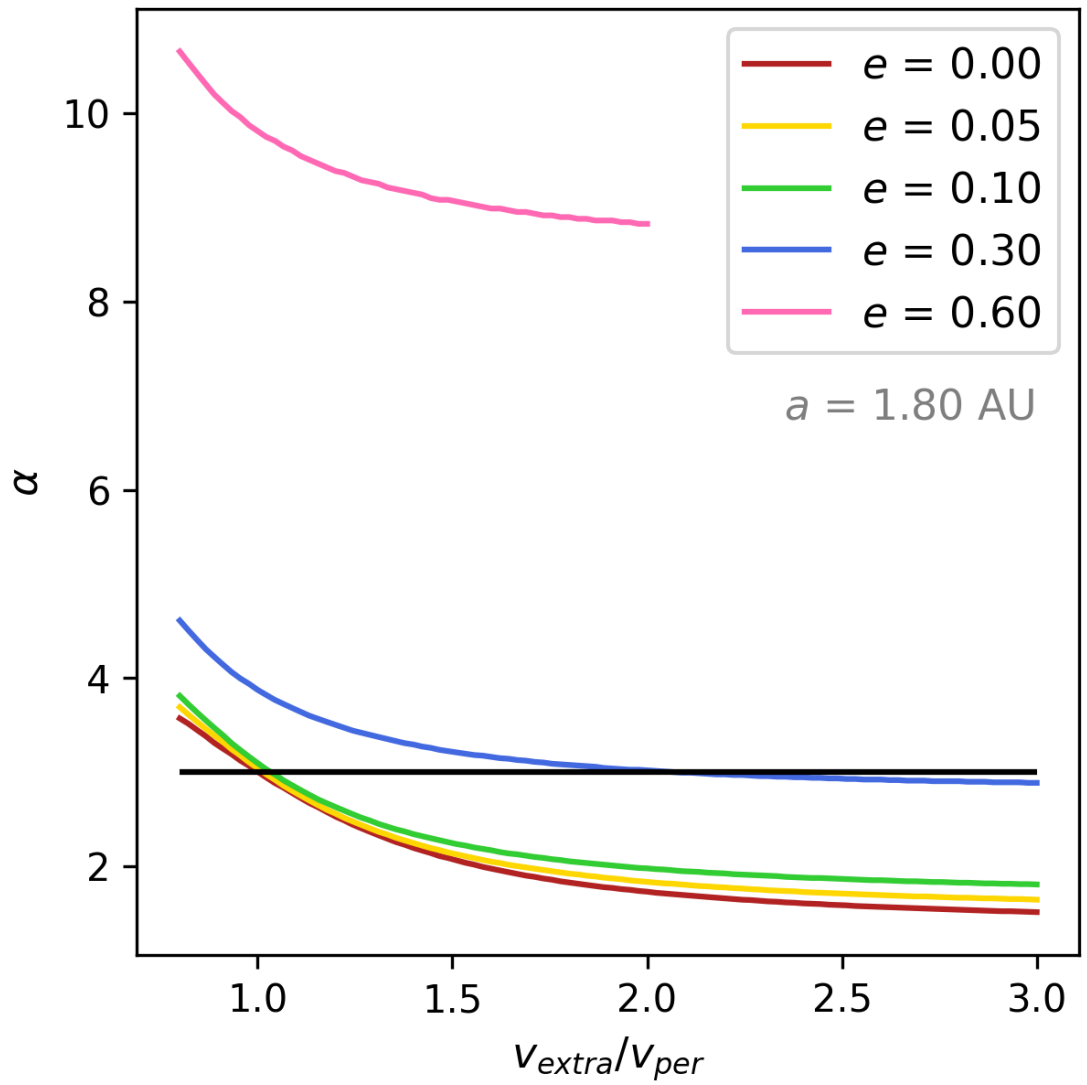

Figure 4.1.1: Ratio of orbital angular momentum to rotational angular momentum at the equillibrium state for a range of values of parameter $v_{\text{extra}}/v_{\text{per}}$. All sistems have $a = 1.80$ AU. Curves for $e = 0.00$, 0.05, 0.10, 0.30 & 0.60 (red, yellow, green, blue & pink) are displayed. It is important to note that we only display the $e = 0.60$ data for $v_{\text{extra}}/v_{\text{per}} < 2$ due to numerical errors related to the computation of $L1$ that were affecting the results.

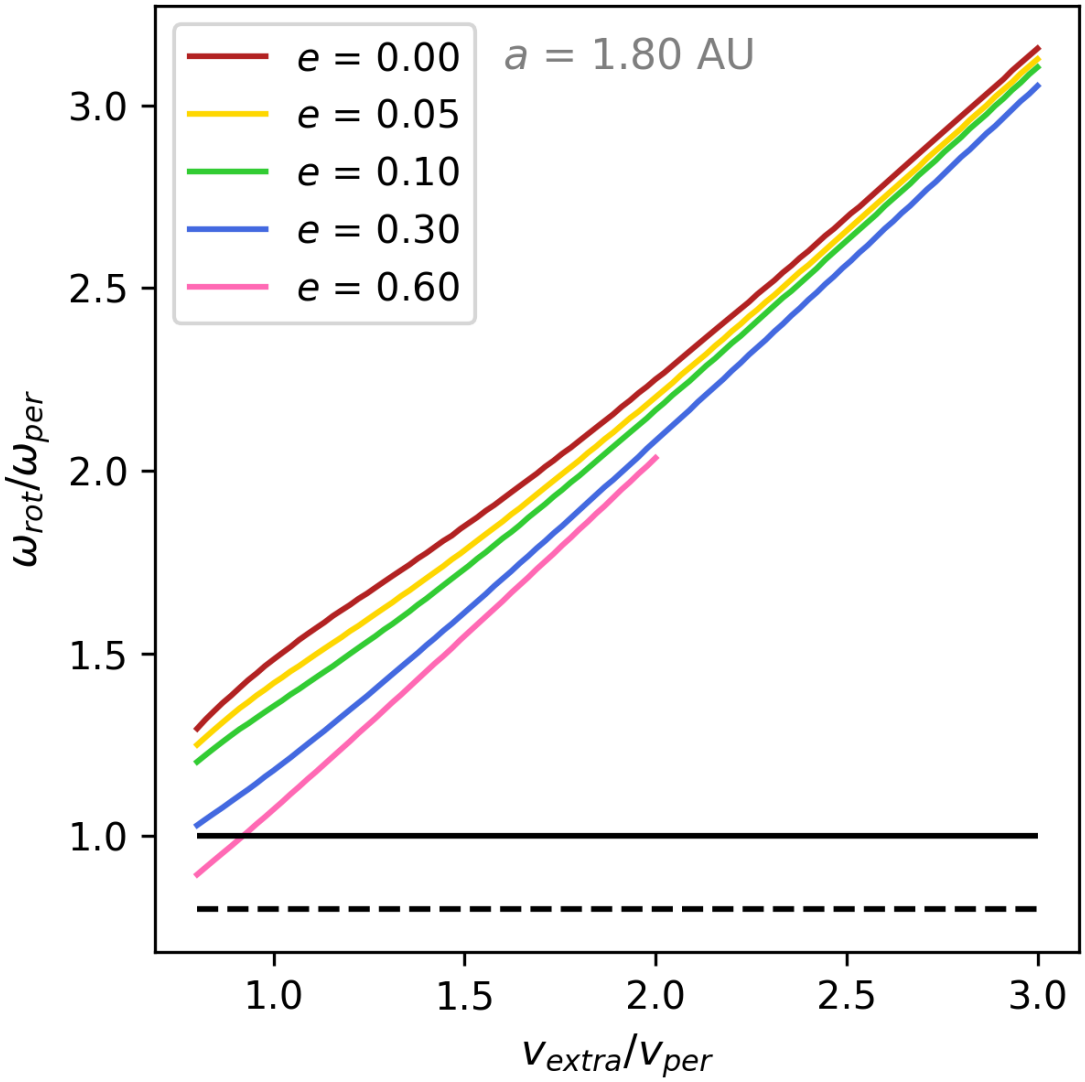

Figure 4.1.2: Akin to figure 2.2.2 but for pseudo-synchronicity. The dashed line and solid black line represent the lower and upper limits for a pseudo-synchronous state (0.8 & 1 respectively). Like in figure 4.1.1, data for $e = 0.60$ is not displayed beyond $v_{\text{extra}}/v_{\text{per}} = 2$ because of numerical issues related to the resolution in the computation of $L1$.

Table 4.1.1: Synchronization ($e = 0.00$) and pseudo-synchronization ($e > 0.00$) times for systems with $a = 1.23$ & 2.30 and $e = 0.00$, 0.30, 0.70 & 0.80, extracted from figure 8 of Moreno et al. (2011). All systems have $\beta_0 = 1.2$ ($v_{\rm extra}/v_{\rm per} = 0.73$).

e	$\tau_{\rm syn}(a = 1.23$ AU) Gyr	$\tau_{\rm syn}(a = 2.30$ AU) Gyr
0.00	3.98×10^5	3.98×10^6
0.30	3.98×10^2	1.58×10^3
0.70	1.58×10^2	3.16×10^2
0.80	1×10^2	2×10^2

of eccentric orbits

$$\tau_{\rm syn}({\rm yr}) = 3.17 \times 10^{38} \frac{m_{\rm don} r_{\rm don}^2 (\beta_0^2 - 1)(1+e)}{\dot{E}_{\rm ave} P (1-e)^3}$$

where P is the orbital period in days, $\dot{E}_{\rm ave}$ is the orbit averaged energy dissipation rate and $m_{\rm don}$ and $r_{\rm don}$ are in solar masses and solar radii respectively. From figure 8 of their work we can get the pseudo-synchronization timescales for systems with eccentricities $e = 0.00$, 0.30, 0.70 & 0.80 and $a = 1.23$ & 2.3 AU (minimum and maximum a values we explore, respectively). These times can be found on table 4.1.1.

Considering it only takes our donor 0.67 Myr to strip its envelope, it is reasonable to think of the donor's rotational velocity as invariable for our timescale.

4.2 Evolution of orbital parameters

Our results show the spin-up effect and mass gain of the accretor after a single orbital period, assuming the semi-major axis and eccentricity of the system remain constant during that span of time. Here, we compare this assumption with previously calculated timescales for changes in a and e, caused by mass transfer.

4.2.1 Semi-major axis a

In both conservative and non-conservative RLOF mass transfer, the mass change can either increase or decrease the orbital separation of the system (Dosopoulou and Kalogera, 2016b).

In Sepinsky et al. (2010), timescales for the evolution of a in systems undergoing

direct accretion are found. The lower rightmost panel of their figure 5 covers our lower eccentricity systems ($0 \leq e \leq 0.10$) but for a slower donor rotation ($f_{1,i} = 0.90 \implies v_{\text{extra}}/v_{\text{per}} < 0.80$ for $e = 0.00$, 0.05, 0.10 & 0.30). Systems with mass ratios of the order of 1 would have a semi-major axis evolution timescale greater than 15 Gyr. Additionally, those systems where $q < 1$ widen, while systems with $q > 1$ experience a shrinkage of their orbit.

For future work, we plan to expand this model to track the evolution of the semi-major axis along with the accretor's spin as consequence of the mass gain so we can get a better understanding of the evolution of eccentric orbits.

4.2.2 Eccentricity e

Meibom and Mathieu (2005) describe the greater orbital period P' for which a binary with the most frequent initial eccentricity in a population circularizes within the lifetimes of the stars, in other words, binary systems with initial periods shorter than P' are expected to have circularized by the age of the population. Their method was tested on eight late-type binary populations with ages ranging from ~ 3 Myr to ~ 10 Gyr. The value of P' increases with the population's age but, for all the discussed cases, does not grow far beyond the value 10 days. The domain of semi-major axis values we explore in this investigation ($\sim 1.25 - 2.30$ AU) result in orbital periods ranging from ~ 340 days to ~ 860 days, much greater than the tidal circularization period of ~ 10 days for populations as old as 10 Gyr. In consequence, we don't expect the eccentricity of our systems to significantly change from their initial values after mass transfer.

The three cases from Hut (1981) we discussed in section 4.1 can also give us some insight on the circularization times: When α is of the order of (greater than) 7, the circularization time will be similar to (greater than) the synchronization time. Since the synchronization times (see table 4.1.1) are many orders of magnitude greater than the time needed for the donor to deplete its envelope, circularization shouldn't be a concern for these cases either. On the other hand, the case where $\alpha - 3 \ll 1$ results in a quicker circularization.

Figure 6 from Sepinsky et al. (2010) presents timescales for the evolution of e. The lower rightmost panel (like in section 4.2.1) covers a parameter space clsoest to ours. There, they obtained an eccentricity evolution timescale lower than 1 Gyr,

however they do note that systems with $e \lesssim 0.05$ could experience an increase in eccentricity instead of circularization.

Overall, the circularization timescales for $e < 0.10$ are larger than our depletion time by many orders of magnitudes and choosing to keep e constant should not present any problem. However, the exact changes in eccentricity for systems with low eccentricities ($e \leq 0.10$) and $v_{\text{extra}}/v_{\text{per}} \sim 1$ remain unconstrained.

4.3 Disk formation

In this work's analysis we have solely focussed on the mass that forms a stream and directly impacts the surface of the accretor. Any mass that did not hit the accretor upon approaching it was count as lost mass while in reality it could still be gravitationally bound to the accretor. If many of these parcels were to continue orbiting the accretor, an accretion disk could form around it.

In future work, we aim to discern between these two cases to better describe scenarios where the formation of an accretion disk can prevent direct accretion by intercepting the stream before it can reach the accretor.

Chapter 5

Conclusion

We presented a novel analytical model to approximate the spin-up effect an accreting star suffers due to direct accretion in a binary system. Our model neglects the effect of the donor's gravitational potential and instead approaches the problem as a particle-accretor two-body system. We explore a range of values of the system's semi-major axis a (1.23 to 2.30 AU), its eccentricity e (0.00 to 0.95) and the donor's rotational velocity $v_{\text{extra}}/v_{\text{per}}$ (0.80 to 1.00).

In regards to the spin-up effect suffered by the accretor star, we find:

1. The maximum spin-up effect we obtain for direct accretion is of the order of 10^{-7} times the accretor's critical rotational velocity, per orbital period. This means that, if the initial orbital parameters were to remain constant, it would take 10^7 periods to spin up the accretor to its critical rotation.

2. For a fixed eccentricity and donor rotational velocity, the spin-up effect is maximized when the semi-major axis equals a_{peak} (see equation 3.1.1). The smaller a is in comparison to a_{peak}, the smaller the contribution to spin-up is. This implies that direct accretion in closer binaries contributes more to the thermal energy of the star than its rotational energy.

3. For a fixed semi-major axis and donor rotational velocity, the dependence on eccentricity can follow one of two trends: If all conditions for direct accretion are satisfied for $e = 0.00$ (case 1), a circular orbit is the most effective at spinning up the accretor. If direct accretion does not occur at $e = 0.00$ (case 2), an orbit is the most effective at spinning up the accretor at the smallest

e for which direct accretion takes place at periastron ($e_{\rm peak}$).

4. For a fixed semi-major axis and eccentricity, the accretor is spun up the most for the smallest $v_{\rm extra}/v_{\rm per}$ value for which direct accretion takes place at periastron. For greater $v_{\rm extra}/v_{\rm per}$ (≤ 1.00), direct accretion becomes more radial and therefore the contribution to rotational (thermal) energy is minimized (maximized).

In regards to mass transfer efficiency for direct accretion:

1. Assuming a, e, $v_{\rm extra}/v_{\rm per}$ and the donor mass loss ratio $\dot{M} = 10^{-6} M_{\odot}/{\rm yr}$ remain constant, it takes the donor between 7.28×10^5 ($a = 1.23$ AU) and 2.85×10^5 ($a = 2.30$ AU) periods (0.67 Myr) to completely shed its envelope. Under the same premise, it would take the accretor around 10^7 periods (9.20 to 23.53 Myr for 1.23 AU $< a <$ 2.30 AU) to reach critical rotation. This implies that, under this premise, the accretor would be able to accrete more than just 10% of its initial mass while avoiding break-up velocity.

2. For a fixed eccentricity and donor rotational velocity, if $a \leq a_{\rm peak}$, all the mass lost by the donor is directly accreted by the accretor. When the opposite is true ($a \geq a_{\rm peak}$) direct accretion only occurs at the farthest point from periastron where the donor is still able to overfill its Roche lobe ($f > 0.00$) and mass is lost around periastron.

3. For a fixed semi-major axis and donor rotational velocity, if all conditions for direct accretion are satisfied for $e = 0.00$, mass transfer is completely conservative for any e (case 1). For case 2, mass transfer is only conservative for $e > e_{\rm peak}$.

4. For a fixed semi-major axis and eccentricity, mass transfer is totally conservative for any $v_{\rm extra}/v_{\rm per}$ value greater than that of the peak in spin-up. When $v_{\rm extra}/v_{\rm per}$ is smaller than that critical value, the mass lost by the donor near periastron is not directly accreted.

We also note that:

1. The maximum spin-up per orbit for systems with $q = 0.50$ and $q = 1.50$ differ in $4 \times 10^{-8} v_{\rm crit}$. Although small, this difference is not negligible when compared to a maximum spin-up of the order of $10^{-7} v_{\rm crit}$. An wider exploration of the parameter space for q will aid us in describing the spin-up's

dependence on the binary's mass ratio.

2. The minimum $v_{\text{extra}}/v_{\text{per}}$ value for direct accretion (~ 0.80 in our model and ~ 1.8 for the three body approach in section 2.2) imply supersynchronization as a requirement for direct accretion. Althought we don't discuss the mechanisms that would cause the donor star to achieve such a rotation rate, we do note that only the outermost layers of the donor are required to be supersynchronous to the orbit.

In adition to the more thoroughly studied a and e effects on accretion, the rotation of the donor seems to also be an imporatl parameter that affects the angle of impact of the accreted mass, influencing the angular momentum transfered to the accretor's rotation. The evolution of the donor's rotation, either through its stellar evolution or through tidal effects, can change the way a system accretes.

Our next step is to track the orbital evolution of the system as a response of mass transfer through our model's prescription so we can better compare with the timescales for a and e in the literature.

In future work, we seek to refine this model by exploring the thermal effects the mass gain can have on the accretor as well as how the depth within the star at which the accreted mass is deposited can influence its properties. We too aim to discern between the lost mass and the parcels that stay bound to the system so we can better describe the whole accretion event in the case an accretion disk forms.

Bibliography

Bate, R. R., Mueller, D. D., White, J. E., and Saylor, W. W. (2020). *Fundamentals of astrodynamics*. Courier Dover Publications.

Chen, Z., Frank, A., Blackman, E. G., Nordhaus, J., and Carroll-Nellenback, J. (2017). Mass transfer and disc formation in AGB binary systems. MNRAS, 468(4):4465–4477.

Counselman, III, C. C. (1973). Outcomes of Tidal Evolution. ApJ, 180:307–316.

Dosopoulou, F. and Kalogera, V. (2016a). Orbital Evolution of Mass-transferring Eccentric Binary Systems. I. Phase-dependent Evolution. ApJ, 825(1):70.

Dosopoulou, F. and Kalogera, V. (2016b). Orbital Evolution of Mass-transferring Eccentric Binary Systems. II. Secular Evolution. ApJ, 825(1):71.

Ferraro, F. R., Mucciarelli, A., Lanzoni, B., Pallanca, C., Cadelano, M., Billi, A., Sills, A., Vesperini, E., Dalessandro, E., Beccari, G., Monaco, L., and Mateo, M. (2023). Fast rotating blue stragglers prefer loose clusters. *Nature Communications*, 14:2584.

Hut, P. (1980). Stability of tidal equilibrium. A&A, 92(1-2):167–170.

Hut, P. (1981). Tidal evolution in close binary systems. A&A, 99:126–140.

Lajoie, C.-P. and Sills, A. (2011). Mass Transfer in Binary Stars Using Smoothed Particle Hydrodynamics. II. Eccentric Binaries. ApJ, 726(2):67.

Leigh, N. W. C., Toonen, S., Portegies Zwart, S. F., and Perna, R. (2020). Mergers of equal-mass binaries with compact object companions from mass transfer in triple star systems. MNRAS, 496(2):1819–1833.

Mathieu, R. D. and Geller, A. M. (2009). A binary star fraction of 76 per cent and unusual orbit parameters for the blue stragglers of NGC 188. Nature, 462(7276):1032–1035.

McClure, R. D. (1984). The barium stars. PASP, 96:117–127.

Meibom, S. and Mathieu, R. D. (2005). A Robust Measure of Tidal Circularization in Coeval Binary Populations: The Solar-Type Spectroscopic Binary Population in the Open Cluster M35. ApJ, 620(2):970–983.

Moreno, E., Koenigsberger, G., and Harrington, D. M. (2011). Eccentric binaries. Tidal flows and periastron events. A&A, 528:A48.

Offner, S. S. R., Moe, M., Kratter, K. M., Sadavoy, S. I., Jensen, E. L. N., and Tobin, J. J. (2023). The Origin and Evolution of Multiple Star Systems. In Inutsuka, S., Aikawa, Y., Muto, T., Tomida, K., and Tamura, M., editors, *Protostars and Planets VII*, volume 534 of *Astronomical Society of the Pacific Conference Series*, page 275.

Packet, W. (1981). On the spin-up of the mass accreting component in a close binary system. A&A, 102(1):17–19.

Pelupessy, F. I., van Elteren, A., de Vries, N., McMillan, S. L. W., Drost, N., and Portegies Zwart, S. F. (2013). The Astrophysical Multipurpose Software Environment. A&A, 557:A84.

Portegies Zwart, S. and Leigh, N. W. C. (2019). A Triple Origin for Twin Blue Stragglers in Close Binaries. ApJ, 876(2):L33.

Portegies Zwart, S. and McMillan, S. (2018). *Astrophysical Recipes; The art of AMUSE*.

Portegies Zwart, S., McMillan, S., Harfst, S., Groen, D., Fujii, M., Nualláin, B. Ó., Glebbeek, E., Heggie, D., Lombardi, J., Hut, P., Angelou, V., Banerjee, S., Belkus, H., Fragos, T., Fregeau, J., Gaburov, E., Izzard, R., Jurić, M., Justham, S., Sottoriva, A., Teuben, P., van Bever, J., Yaron, O., and Zemp, M. (2009). A multiphysics and multiscale software environment for modeling astrophysical systems. New A, 14(4):369–378.

Portegies Zwart, S., McMillan, S. L. W., van Elteren, E., Pelupessy, I., and de Vries, N. (2013). Multi-physics simulations using a hierarchical interchangeable software interface. *Computer Physics Communications*, 184(3):456–468.

Raghavan, D., McAlister, H. A., Henry, T. J., Latham, D. W., Marcy, G. W., Mason, B. D., Gies, D. R., White, R. J., and ten Brummelaar, T. A. (2010). A Survey of Stellar Families: Multiplicity of Solar-type Stars. ApJS, 190(1):1–42.

Sandage, A. R. (1953). The color-magnitude diagram for the globular cluster M 3. AJ, 58:61–75.

Sepinsky, J. F., Willems, B., Kalogera, V., and Rasio, F. A. (2007). Interacting Binaries with Eccentric Orbits: Secular Orbital Evolution Due to Conservative Mass Transfer. ApJ, 667(2):1170–1184.

Sepinsky, J. F., Willems, B., Kalogera, V., and Rasio, F. A. (2009). Interacting Binaries with Eccentric Orbits. II. Secular Orbital Evolution due to Non-conservative Mass Transfer. ApJ, 702(2):1387–1392.

Sepinsky, J. F., Willems, B., Kalogera, V., and Rasio, F. A. (2010). Interacting Binaries with Eccentric Orbits. III. Orbital Evolution due to Direct Impact and Self-Accretion. ApJ, 724(1):546–558.

Valtonen, M. and Karttunen, H. (2006). *The planar restricted circular three-body problem and other special cases*, page 115–140. Cambridge University Press.

Appendix A

Apendix

A1 Limits on v_{extra}/v_{per}

At periastron, a particle is shed from a donor star's envelope and falls from a distance r_{L1}, onto a central body of mass m_{acc}, with an initial velocity v_i. This particle will move on an orbit of eccentricity e_p and semi-major axis a_p. If v_i is perpendicular to the direction of the initial position of the particle $\vec{r}_{L1}$, this starting position must be either the periapsis or apoapsis of its orbit. Taking assumption I into consideration, an initial velocity equal to

$$v_i = \sqrt{\frac{Gm_{acc}}{r_{L1}}} \tag{A1.1}$$

will result in a circular orbit. For lower velocities, the parcel's orbit will shrink, decreasing its semi-major axis and become more eccentric, making the initial position at r_{L1} the apoapsis of the orbit:

$$r_{p,apo} = r_{L1} \tag{A1.2}$$

We then locate the center of mass of the central body which corresponds to the foci closest to periapsis. If the central body were to have a radius r_{acc}, the particle would impact onto the central body's surface when

$$r_{p,per} \leq r_{acc} \tag{A1.3}$$

where $r_{p,per}$ is the particle's periapsis distance. In turn, given equation A1.2 and the highest possible value for $r_{p,per}$ in expression A1.3, the greatest length of the semi-major axis of the particle's orbit so that it still impacts the central body is

$$a_p = \frac{r_{acc} + r_{L1}}{2} \tag{A1.4}$$

Replacing this within the vis-viva equation (2.1.4), we obtain the minimum initial velocity required for an orbit that impacts the central body

$$v_i = \sqrt{\frac{2Gm_{acc}}{r_{L1} + r_{L1}^2/r_{acc}}} \tag{A1.5}$$

This configuration is exemplified by figure A1.1.

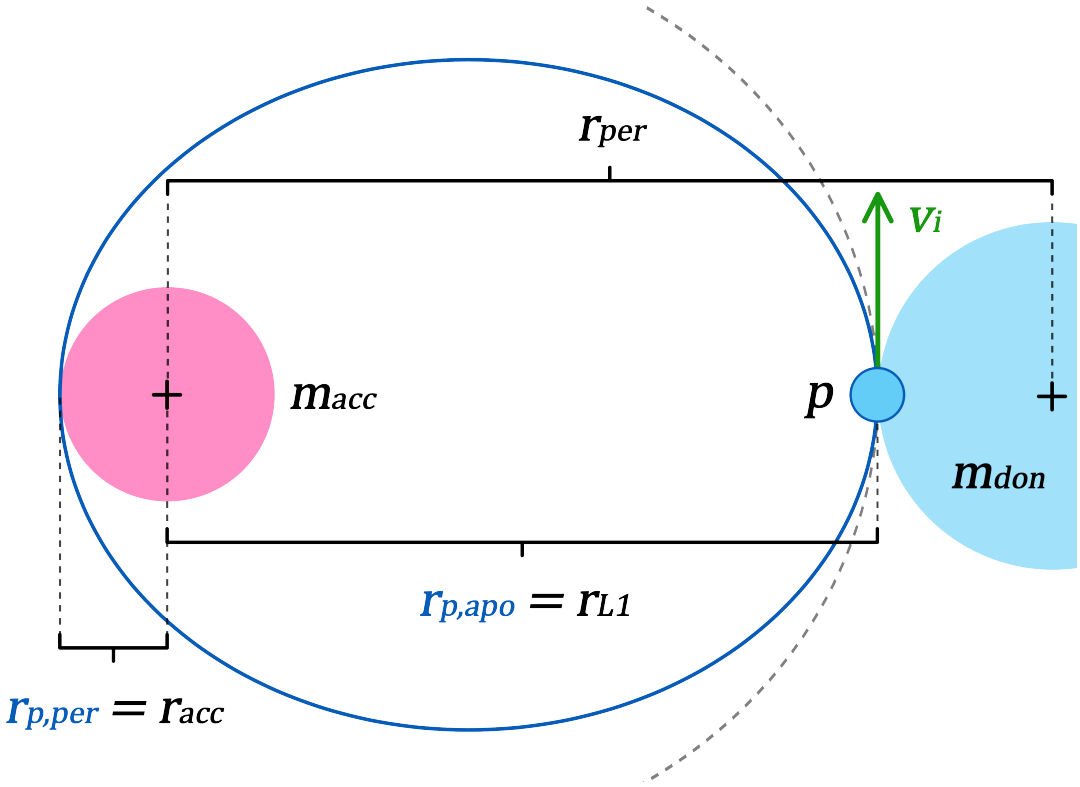

Figure A1.1: Caption

From equation 2.1.2, we know that at periastron, where the orbital and extra velocity are perpendicular to each other, the particle's initial velocity will be given by

$$v_i = v_{per} - v_{extra} \tag{A1.6}$$

where v_{per} is the velocity of the donor star around the accretor star at periastron. This velocity can be obtained through the vis-viva equation (2.1.4)

$$v_{per} = \sqrt{G(m_{acc} + m_{don}) \left(\frac{2}{r_{per}} - \frac{1}{a} \right)} \tag{A1.7}$$

Dividing equation A1.6 by v_{per} and replacing A1.5 and A1.6, we obtain an expression for the lowest value the synchronicity parameter v_{extra}/v_{per} can take to ensure direct accretion occurs

$$\frac{v_{extra}}{v_{per}} = 1 - \sqrt{\frac{2m_{acc}}{(r_{L1} + r_{L1}^2/r_{acc})(m_{acc} + m_{don})(2/r_{per} - 1/a)}} \tag{A1.8}$$

$$v_i = v_{per} \left(1 - \frac{v_{extra}}{v_{per}} \right) \tag{A1.9}$$

$$\frac{Gm_{don}}{(r_{per} - r_{L1})^2} - \frac{Gm_{acc}}{r_{L1}^2} + \frac{2Gm_{acc}}{r_{L1}^2 + r_{L1}^3/r_{acc}} = 0 \tag{A1.10}$$

A2 Eccentricity and angular momentum

In section 2, equation 2.1.6 provides the eccentricity from the geometrical components of an ellipse a and c. Here, we will demonstrate that this expression agrees with the conservation of angular momentum.

In terms of angular momentum, the eccentricity of an orbit can be written as

$$e = \sqrt{1 + \frac{2EL^2}{m_{\text{rdc}}\gamma}} \tag{A2.1}$$

where E is the total orbital energy, L is the angular momentum, m_{rdc} is the reduced mass

$$m_{\text{rdc}} = \frac{m_1 m_2}{m_1 + m_2}$$

and γ is the coefficient of the inverse-square law central force. Bate et al. (2020)

rewrite this equation for the case of a central gravitational force

$$e = \sqrt{1 + \frac{2\epsilon h^2}{\mu^2}} \tag{A2.2}$$

where ϵ is the specific orbital energy

$$\epsilon = -\frac{\mu}{2a}$$

, h is the specific angular momentum

$$\vec{h} = \vec{r} \times \vec{v}$$

and μ is the standard gravitational parameter

$$\mu = G(m_1 + m_2)$$

Replacing with the particle's initial conditions $\vec{r} = r_{L1}\hat{r}$, $\vec{v} = v_{i,r}\hat{r} + v_{i,\theta}\hat{\theta}$, $a = a_p$ and $\mu = Gm_{\text{acc}}$, equation A2.2 can be rewritten as

$$e_p = \sqrt{1 - \frac{r_{L1} v_i^2 \sin(\alpha_i)}{G a_p m_{\text{acc}}}} \tag{A2.3}$$

Our goal now is to equate expression 2.1.6 to expression A2.3.

If we replace expression 2.1.7 into equation 2.1.6, we get

$$\begin{aligned} e_p &= \frac{1}{2}\sqrt{r_{L1}^2 + (2a_p - r_{L1})^2 - 2r_{L1}(2a_p - r_{L1})\cos(\pi - 2\alpha_i)}\frac{1}{a_p} \\ &= \frac{1}{2}\sqrt{\frac{r_{L1}^2}{a_p^2} + \frac{(2a_p - r_{L1})^2}{a_p^2} - \frac{2r_{L1}(2a_p - r_{L1})\cos(\pi - 2\alpha_i)}{a_p^2}} \\ &= \frac{1}{2}\sqrt{\frac{r_{L1}^2}{a_p^2} + 4 - 4\frac{r_{L1}}{a_p} + \frac{r_{L1}^2}{a_p^2} - \left(4\frac{r_{L1}}{a_p} - 2\frac{r_{L1}^2}{a_p^2}\right)\cos(\pi - 2\alpha_i)} \end{aligned}$$

We can rearange the Vis-viva equation (equation 2.1.4) as

$$\frac{r_{L1}}{a_p} = 2 - \frac{r_{L1} v_i^2}{G m_{\text{acc}}} \tag{A2.4}$$

If we replace A2.4 in the previous equation and define

$$k = \frac{r_{L1} v_i^2}{G m_{\rm acc}} \tag{A2.5}$$

we obtain

$$\begin{aligned} e_p &= \frac{1}{2}\sqrt{(2-k)^2 + 4 - 4(2-k) + (2-k)^2 - [4(2-k) - 2(2-k)^2]\cos(\pi - 2\alpha_i)} \\ &= \frac{1}{2}\sqrt{2k^2 - 4k + 4 - (-2k^2 + 4k)\cos(\pi - 2\alpha_i)} \\ &= \frac{1}{2}\sqrt{(2k^2 - 4k) + (2k^2 - 4k)\cos\left[2\left(\frac{\pi}{2} - \alpha_i\right)\right] + 4} \end{aligned}$$

We can now rewrite the cosine as

$$\begin{aligned} \cos\left[2\left(\frac{\pi}{2} - \alpha_i\right)\right] &= \cos^2\left(\frac{\pi}{2} - \alpha_i\right) - \sin^2\left(\frac{\pi}{2} - \alpha_i\right) \\ &= 1 - \sin^2\left(\frac{\pi}{2} - \alpha_i\right) - \sin^2\left(\frac{\pi}{2} - \alpha_i\right) \\ &= 1 - 2\sin^2\left(\frac{\pi}{2} - \alpha_i\right) \end{aligned}$$

, then

$$\begin{aligned} e_p &= \frac{1}{2}\sqrt{(2k^2 - 4k) + (2k^2 - 4k)\left[1 - 2\sin^2\left(\frac{\pi}{2} - \alpha_i\right)\right] + 4} \\ &= \frac{1}{2}\sqrt{(2k^2 - 4k) + (2k^2 - 4k)\left[1 - 2\sin^2\left(\frac{\pi}{2} - \alpha_i\right)\right] + 4} \\ &= \frac{1}{2}\sqrt{(2k^2 - 4k) + (2k^2 - 4k) - 2(2k^2 - 4k)\sin^2\left(\frac{\pi}{2} - \alpha_i\right) + 4} \\ &= \frac{1}{2}\sqrt{4(k^2 - 2k) - 4(k^2 - 2k)\sin^2\left(\frac{\pi}{2} - \alpha_i\right) + 4} \\ &= \sqrt{(k^2 - 2k) - (k^2 - 2k)\sin^2\left(\frac{\pi}{2} - \alpha_i\right) + 1} \\ &= \sqrt{(k-1)^2 - (k^2 - 2k)\sin^2\left(\frac{\pi}{2} - \alpha_i\right)} \end{aligned}$$

Replacing

$$\begin{aligned} \sin\left(\frac{\pi}{2} - \alpha_i\right) &= \sin\left(\frac{\pi}{2}\right)\cos\alpha_i - \cos\left(\frac{\pi}{2}\right)\sin\alpha_i \\ &= \cos\alpha_i \end{aligned}$$

we get

$$\begin{aligned} e_p &= \sqrt{(k-1)^2 - (k^2-2k)\cos^2\alpha_i} \\ &= \sqrt{(k-1)^2 + (2k-k^2)(1-\sin^2\alpha_i)} \\ &= \sqrt{k^2 - 2k + 1 + 2k - k^2 - (2k-k^2)\sin^2\alpha_i} \\ &= \sqrt{1 - k(2-k)\sin^2\alpha_i} \end{aligned}$$

We remember than from equation A2.4, $r_{L1}/a_p = 2 - k$. Then

$$e_p = \sqrt{1 - k\frac{r_{L1}}{a_p}\sin^2\alpha_i}$$

Finally, replacing k with equation A2.5, we obtain

$$e_p = \sqrt{1 - \frac{r_{L1}v_i^2\sin(\alpha_i)}{Ga_p m_{\text{acc}}}} \tag{A2.6}$$